The D50N mutation and syndromic deafness: Altered Cx26 hemichannel properties caused by effects on the pore and intersubunit interactions

Helmuth A. Sanchez,[1] Krista Villone,[2] Miduturu Srinivas,[2] and Vytas K. Verselis[1]

[1]Dominick P. Purpura Department of Neuroscience, Albert Einstein College of Medicine, Bronx, NY 10461
[2]Department of Biological Sciences, State University of New York College of Optometry, New York, NY 10036

Mutations in the *GJB2* gene, which encodes Cx26, are the most common cause of sensorineural deafness. In syndromic cases, such as keratitis-ichthyosis-deafness (KID) syndrome, in which deafness is accompanied by corneal inflammation and hyperkeratotic skin, aberrant hemichannel function has emerged as the leading contributing factor. We found that D50N, the most frequent mutation associated with KID syndrome, produces multiple aberrant hemichannel properties, including loss of inhibition by extracellular Ca^{2+}, decreased unitary conductance, increased open hemichannel current rectification and voltage-shifted activation. We demonstrate that D50 is a pore-lining residue and that negative charge at this position strongly influences open hemichannel properties. Examination of two putative intersubunit interactions involving D50 suggested by the Cx26 crystal structure, K61–D50 and Q48–D50, showed no evidence of a K61–D50 interaction in hemichannels. However, our data suggest that Q48 and D50 interact and disruption of this interaction shifts hemichannel activation positive along the voltage axis. Additional shifts in activation by extracellular Ca^{2+} remained in the absence of a D50–Q48 interaction but required an Asp or Glu at position 50, suggesting a separate electrostatic mechanism that critically involves this position. In gap junction (GJ) channels, D50 substitutions produced loss of function, whereas K61 substitutions functioned as GJ channels but not as hemichannels. These data demonstrate that D50 exerts effects on Cx26 hemichannel and GJ channel function as a result of its dual role as a pore residue and a component of an intersubunit complex in the extracellular region of the hemichannel. Differences in the effects of substitutions in GJ channels and hemichannels suggest that perturbations in structure occur upon hemichannel docking that significantly impact function. Collectively, these data provide insight into Cx26 structure–function and the underlying bases for the phenotypes associated with KID syndrome patients carrying the D50N mutation.

The Journal of General Physiology

INTRODUCTION

Cx26, one of 20 connexins in the human genome, is expressed in keratinocytes and in support cells of the inner ear. Over 100 mutations in the Cx26 gene, *GJB2*, have been identified that cause sensorineural deafness, but a small subset of these are linked to syndromes, such as keratitis-ichthyosis-deafness (KID) and palmoplantar keratoderma, in which deafness is accompanied by severe hyperkeratotic, inflammatory skin disorders (Hoang Dinh et al., 2009; Lee and White, 2009). Mutations associated with syndromic deafness are all missense mutations of single residues, and evidence points to aberrantly behaving, undocked Cx26 hemichannels rather than dysfunctional gap junction (GJ) channels as the principal underlying basis of disease (Stong et al., 2006; Gerido et al., 2007; Lee et al., 2009; Sánchez et al., 2010; Terrinoni et al., 2010). The aberrant behavior generally has been described by the term "leaky" to indicate increased opening of hemichannels in the plasma membrane. Being a large ion channel, increased opening of Cx26 hemichannels can substantively alter cellular physiology and, when excessive, severely compromise cellular integrity.

Among the 10 mutations in Cx26 that have been linked to KID, D50N is the most common (Mazereeuw-Hautier et al., 2007; Lee and White, 2009) and produces moderate to profound hearing loss that is accompanied by hyperkeratosis, sparse scalp hair, dystrophic nails, corneal dystrophy, and keratitis (Richard et al., 2002; van Steensel et al., 2002; Yotsumoto et al., 2003; Janecke et al., 2005). Initial analysis of the D50N mutant expressed in *Xenopus laevis* oocytes showed marked dysregulation of hemichannels by extracellular Ca^{2+}, which could lead to increased hemichannel opening in the plasma membrane (Lee et al., 2009). In addition, D50N failed to induce functional coupling between cells (Lee et al., 2009). D50 is located in the first extracellular loop domain, E1, and thus, it has been suggested that the D50N mutation could alter GJ channel gating and/or affect hemichannel interactions, e.g., docking

Correspondence to Vytas K. Verselis: vytas.verselis@einstein.yu.edu

Abbreviations used in this paper: GJ, gap junction; KID, keratitis-ichthyosis-deafness; ME, 2-mercaptoethanol; S4SM, stochastic four-state model; SCAM, substituted Cys accessibility method.

The Rockefeller University Press $30.00
J. Gen. Physiol. Vol. 142 No. 1 3–22
www.jgp.org/cgi/doi/10.1085/jgp.201310962

(Richard et al., 2002; van Steensel et al., 2002; Yotsumoto et al., 2003). However, studies of Cx46 and Cx50 hemichannels identified this homologous position, D51, to be pore lining (Kronengold et al., 2003; Verselis et al., 2009) using the substituted Cys accessibility method (SCAM). Assignment of D50 to the pore of Cx26 is also supported by the crystal structure of the Cx26 GJ channel (Maeda et al., 2009).

Here we examine D50N mutant hemichannels at macroscopic and single hemichannel levels and find several altered properties in addition to Ca^{2+} dysregulation. These properties include a substantially reduced unitary conductance, increased open-state outward rectification, and strongly shifted voltage-dependent activation. Application of SCAM confirmed D50 as a pore-lining residue in Cx26 hemichannels. Interestingly, the Cx26 crystal structure suggests that D50 not only lines the pore, but also participates in intersubunit interactions. In this study, we explore the putative intersubunit interactions involving D50 and their role in Ca^{2+} regulation and voltage-dependent gating of Cx26 hemichannels.

MATERIALS AND METHODS

Construction of Cx26 mutants

Human WT Cx26 was cloned into the BamHI restriction site of the $pCS2^{+}$ expression vector for functional experiments in *Xenopus* oocytes and Neuro-2a (N2A) cells. G45E and A40V mutants were prepared as previously described (Gerido et al., 2007; Sánchez et al., 2010). The Cx50 coding sequence was subcloned into the SP64T transcription vector (provided by T. White, State University of New York at Stony Brook, Stony Brook, NY). All site-directed mutations were constructed using the QuikChange mutagenesis kit (Agilent Technologies) in accordance with the manufacturer's protocol using the WT connexin expression constructs as templates. All constructs were verified by sequencing.

Exogenous expression of connexins

For expression of connexins in *Xenopus* oocytes, RNA was synthesized and oocytes were prepared and injected as previously described (Trexler et al., 1996, 2000). Injected oocytes were maintained at 16–18°C in a modified ND96 solution containing (in mM) 100 NaCl, 2 KCl, 1 $MgCl_2$, 1.8 $CaCl_2$, 10 glucose, 10 HEPES, and 5 pyruvate, pH adjusted to 7.6. For expression of connexins in mammalian cells, N2A cells were transiently cotransfected with Cx cDNA and a pmCherry vector (Takara Bio Inc.) using Lipofectamine 2000 reagent (Invitrogen) as previously described (Srinivas et al., 2001).

Reagents

The MTS reagents, 2-trimethylammonioethylmethanethiosulfonate (MTSET) and 2-sulfonatoethylmethanethiosulfonate (MTSES) were purchased from Anatrace. 2-(6-biotinoylaminohexanoylamino)ethylmethanethiosulfonate (MTSEA biotin-X) was purchased from Biotium. Aliquots of dry powder were prepared and stored in microcentrifuge tubes at −20°C. Before each experiment, aliquots of MTSET and MTSES were dissolved in distilled water, chilled on ice, to stock concentrations of 200 mM. Dilutions were made into appropriate perfusion solutions just before application to a final concentration of 0.2 mM for MTSET and 2 mM for MTSES. MTSEA biotin-X was dissolved in DMSO to a stock concentration of 200 mM and diluted to a concentration of 0.2 mM. Activity of MTS reagents were periodically checked using the TNB assay (Karlin and Akabas, 1998).

Macroscopic electrophysiological recording

Macroscopic hemichannel currents in *Xenopus* oocytes were recorded as previously described (Sánchez et al., 2010). In brief, oocytes were placed in a polycarbonate RC-1Z recording chamber (Warner Instruments) with inflow and outflow compartments. The outflow compartment contained agar bridges connected to a VG-2A virtual ground bath clamp (Molecular Devices). All recordings were obtained with a GeneClamp 500 two-electrode voltage clamp (Molecular Devices). Both current-passing and voltage-recording pipettes contained 1 M KCl. During recording, oocytes were perfused with simple salt solutions that contained (in mM) 100 NaCl, 1 $MgCl_2$, and 10 HEPES, to which Ca^{2+} concentration was adjusted to desired levels. A 0 Ca^{2+} solution refers to a nominal condition in which no $CaCl_2$ was added. Conductance measurements in high and low Ca^{2+} conditions were obtained from voltage step and voltage ramp protocols that are described in the figure legends.

Mutant cycle analysis

Mutant cycle analysis (Yifrach and MacKinnon, 2002; DeCaen et al., 2008) was performed on the voltage and Ca^{2+} dependence of loop gating using WT, Q48A, D50A, and Q48A + D50A hemichannels. To assess gating parameters, I-V curves were obtained from a voltage ramp protocol that consisted of a voltage step to 40 mV from a holding potential of −20 mV for 30 s to allow hemichannels to reach steady-state, followed by a slow (600 s) voltage ramp to −100 mV. Currents were filtered at 200 Hz and data were acquired at 2 kHz. G-V curves were calculated from $G = I/(V - V_r)$, where V_r is the reversal potential, and fit to a stochastic four-state model (S4SM) of voltage gating of GJ channels (Paulauskas et al., 2009) adapted for hemichannels by eliminating the influence of one hemichannel from the S4SM fitting algorithm. The model accounts for the unitary conductance of the hemichannel, its open state I-V relation, and three parameters characterizing gating: polarity, whether closure occurs for hyperpolarization or depolarization, $V_{1/2}$, the voltage at which the open probability is 0.5, and A, the steepness voltage dependence expressed as zF/RT, where z is the apparent gating charge and F, R, and T have their usual meanings. To assess rectification associated with the open state of a hemichannel, we applied a series of brief voltage steps from 40 to −100 mV from a holding potential of −20 mV. These steps were applied in 0 (nominal) and 2 mM extracellular Ca^{2+} for WT and each mutant hemichannel. The initial currents were measured to obtain open hemichannel G-V relationships that were fit to exponential functions. These functions were used when fitting G-V curves obtained from ramps to obtain gating parameters. We used an Exkor algorithm of global optimization to fit experimental G-V plots (see Paulauskas et al. [2012]). During the fitting process for WT Cx26 and mutant hemichannels, we assumed that only the loop gate was functional. This assumption is supported by single hemichannel data essentially showing only loop gating been 40 and −100 mV (see Fig. 5).

For WT and each mutant, we calculated ΔG^0, the chemical free energy difference between open and closed states, from $-zFV_{1/2}/RT$ using values for z and $V_{1/2}$ obtained from the fits using the S4SM. The change in free energy of each mutant relative to WT was calculated as $\Delta(\Delta G^0)_{mut} = -F(z_{mut}V_{1/2\,mut} - z_{WT}V_{1/2\,WT})$. The Q48–D50 coupling energy was calculated as $\Delta G_{coupling} = (\Delta G^0_{D50A} - \Delta G^0_{WT}) - (\Delta G^0_{D50A+Q48A} - \Delta G^0_{Q48A})$.

Single hemichannel recording

For patch-clamp recordings of single hemichannel currents, *Xenopus* oocytes were manually devitellinized in a hypertonic solution

consisting of (in mM) 220 Na Aspartate, 10 KCl, 2 $MgCl_2$, and 10 HEPES and then placed in the ND96 solution for recovery. Oocytes were then individually moved to a recording chamber (RC-28; Warner Instruments Corp.) containing the patch pipette solution (IPS) which consisted of (in mM) 140 KCl, 1 $MgCl_2$, 5 HEPES, 1 $CaCl_2$, and 3 EGTA, pH adjusted to 8.0 with KOH. The bath compartment was connected via a 3-M agar bridge to a ground compartment containing the same IPS solution. After excision of patches, hemichannels were exposed to symmetric solutions, and any instrumentation offsets were manually corrected in the absence of an applied voltage. Single hemichannel I-V curves were obtained by applying 8-s voltage ramps from −70 to 70 mV. Currents were leak-subtracted by measuring leak conductance of a given patch from full closing transitions and extrapolating linearly over the entire voltage range. Because single hemichannel currents were not linear with voltage, conductance was measured as the slope conductance obtained from linear fits of leak-subtracted currents at ∼0 mV. In experiments examining accessibility to MTS reagents, patches were excised in inside-out and outside-out configurations, to which MTS reagents were applied by addition to the bath. Single hemichannel I-V curves were obtained before and after MTS application. Currents were typically filtered at 1 kHz, and data were acquired at 5 kHz.

Recordings of GJ currents

For measurements of junctional conductance (g_j) in *Xenopus* oocytes, cells were manually devitellinized and paired by placing them in dishes coated with 1% agarose. Each oocyte of a pair was clamped independently using a two-electrode voltage clamp to a common potential (typically −40 mV). V_j steps, 10 s in duration, were applied by stepping the voltage in one cell of a pair over a range of ±120 mV in 10-mV increments; the voltage in the other cell remained constant. Each V_j step was preceded by a small, brief prepulse of constant amplitude (10 mV) so that a family of currents could be normalized if the expression level changed over the course of an experiment. The cells were allowed to recover for 60 s between V_j steps. Currents were filtered at 200 Hz and digitized at 1–2 kHz. Steady-state currents were obtained by extrapolating exponential fits of the data to t = 0 and t = ∞ as previously described (Verselis et al., 1994). Only cell pairs with g_j values ≤5 µS were used to avoid effects of series access resistance on voltage dependence (Wilders and Jongsma, 1992).

In transfected N2A cells, g_j was measured between cell pairs by using the dual whole cell voltage clamp technique with Axopatch 1D patch-clamp amplifiers (Axon Instruments) at room temperature. The solution bathing the cells contained (in mM) 140 NaCl, 5 KCl, 2 CsCl, 2 $CaCl_2$, 1 $MgCl_2$, 5 HEPES, 5 dextrose, 2 pyruvate, and 1 $BaCl_2$, pH 7.4. Patch electrodes had resistances of 3–5 MΩ when filled with internal solution containing (in mM) 130 CsCl, 10 EGTA, 0.5 $CaCl_2$, and 10 HEPES, pH 7.2. Macroscopic and single channel recordings were filtered at 0.2–0.5 kHz and sampled at 1–2 kHz. Single channel currents were investigated in weakly coupled cell pairs (one or two channels) without the use of uncoupling agents by applying voltage pulses to one cell of a pair.

Acquisition of electrophysiological data

In electrophysiological experiments using oocytes, data were acquired with AT-MIO-16X D/A boards from National Instruments using custom acquisition software (written by E.B. Trexler, Gotham Scientific). For N2A cells, data were acquired by using PCLAMP8 software (Axon Instruments); analysis was performed with PCLAMP8 and ORIGIN 6.0 software (Microcal Software).

Western blots

We used previously described protocols for Westerns blots (White et al., 1992; Meşe et al., 2004) with some modifications. In brief, oocytes were washed two times with PBS solution without added $CaCl_2$ and resuspended in lysis buffer containing 5 mM Tris-HCl, pH 8.0, 5 mM EDTA, 5 mM EGTA, and protease inhibitors (1 mg/ml benzamidine, 1 mg/ml ε-aminocaproic acid, and 2 mM PMSF) and phosphatase inhibitors (20 mM $Na_4P_2O_7$). Then, oocytes were sheared at 4°C using a 3-ml syringe with a 23-gauge needle, followed by sonication with an ultrasonic processor (S-4000; MISONIX). After homogenization, yolk and debris were centrifuged at 1,000 *g* at 4°C for 5 min in a microcentrifuge, and the supernatant was transferred and centrifuged at 100,000 *g* (38,200 rpm) at 4°C for 30 min in a Beckman Coulter (rotor SW55i) ultracentrifuge. Membrane pellets were dissolved in 50 µl of a buffer solution (20 mM Tris-HCl, 2 mM EDTA, 1 mM EGTA, 1% [wt/vol] SDS, and 1% [vol/vol] Triton X-100, pH 7.4) and incubated under agitation at 4°C for 30 min. Then, 40 µl Laemmli buffer with or without 10% (vol/vol) 2-mercaptoethanol (ME) and 10 mM DTT was added. The samples were immediately loaded onto 12% acrylamide gels.

After electrophoresis, proteins were electrotransferred to nitrocellulose membranes. Nonspecific protein binding was blocked by incubation of the nitrocellulose membranes in PBS-BLOTTO (5% skim milk in PBS solution) for 40 min. The membranes were then incubated overnight with a polyclonal anti-Cx26 antibody (Life Technologies) at a 1:1,000 dilution, followed by several washes with PBS, and incubated with antibody conjugated with horseradish peroxidase (Life Technologies) at a 1:2,000 dilution. The immunoenhanced chemiluminescence was detected with the West Dura SuperSignal kit (Thermo Fisher Scientific) according to the manufacturer's instructions. The resulting immunoblots were scanned with a CanoScan LiDE scanner (Canon Inc.).

RESULTS

D50N hemichannels and sensitivity to extracellular Ca^{2+}

Connexin hemichannels generally show robust inhibition by extracellular Ca^{2+}. Fig. 1 A shows examples of a families of hemichannel currents recorded in 0.2, 2, and 5 mM extracellular Ca^{2+} for WT Cx26, D50N, and the two additional KID mutants, G45E and A40V, that are also located in the proximal portion of the first extracellular loop, E1, near its border with the first transmembrane domain, the TM1/E1 border. Both A40V and G45E hemichannels, like WT Cx26 hemichannels, continue to show inhibition by Ca^{2+}, with currents substantially reduced in 2 mM Ca^{2+} compared with 0.2 mM Ca^{2+}. Raising Ca^{2+} to 5 mM produced further reductions in current. At the higher Ca^{2+} concentrations, G45E hemichannels showed activation of Ca^{2+}-dependent Cl currents at −110 mV after steps to positive voltages as a result of increased Ca^{2+} permeability giving rise to a biphasic current superimposed on the tail current as previously reported (Sánchez et al., 2010). However, D50N hemichannels were poorly sensitive to Ca^{2+}, with currents changing little over the same range of extracellular Ca^{2+} concentrations.

Inhibition by Ca^{2+} was quantified by plotting the ratio of the macroscopic conductances measured in 2 and 0.2 mM Ca^{2+}, $G_{2Ca^{2+}}/G_{0.2Ca^{2+}}$ (Fig. 1 B). WT Cx26 exhibited a conductance ratio of ∼0.1, whereas A40V exhibited modest weakening of inhibition by Ca^{2+}, and G45E

behaved similar to WT Cx26, consistent with our previously published study (Sánchez et al., 2010). However, D50N exhibited a near loss of Ca^{2+} sensitivity with a conductance ratio of ∼0.8. Given that these data only represent a snapshot of Ca^{2+} regulation at a single voltage, we examined inhibition by Ca^{2+} over a wide voltage range (Fig. 1 C). Conductance ratios are shown in 2 and 0.2 mM Ca^{2+} ranging from 40 to −80 mV calculated from G-V relationships obtained from slow voltage ramps. Ca^{2+} dysregulation for G45E emerged at positive voltages and over a wider voltage range for A40V. However, D50N stood out, exhibiting poor inhibition by Ca^{2+} over the entire voltage range.

D50N single hemichannel currents

Fig. 2 shows examples of unitary hemichannel currents for WT Cx26 and D50N obtained in response to voltage ramps. The recordings were obtained from excised patches in which both the bath and pipette solutions consisted of 140 mM KCl as the principal salt with EGTA added to chelate Ca^{2+} to submicromolar levels. The unitary conductance of D50N, measured as the slope conductance at 0 mV, was found to be considerably smaller than WT Cx26. Mean slope conductance was 167 ± 13 pS (n = 16) compared with 358 ± 23 pS (n = 18) for WT Cx26. In addition, the open D50N hemichannel current exhibited robust outward rectification with current approximately threefold larger at 70 mV than at −70 mV. WT Cx26 exhibited only a slight outward rectification, with an ∼1.2-fold larger current at 70 mV compared with −70 mV. These changes in unitary conductance and open hemichannel rectification associated with D50N can be explained by a location in the aqueous pore at the extracellular end, as suggested by the Cx26 crystal structure (Maeda et al., 2009) and inferred by SCAM studies of this homologous position

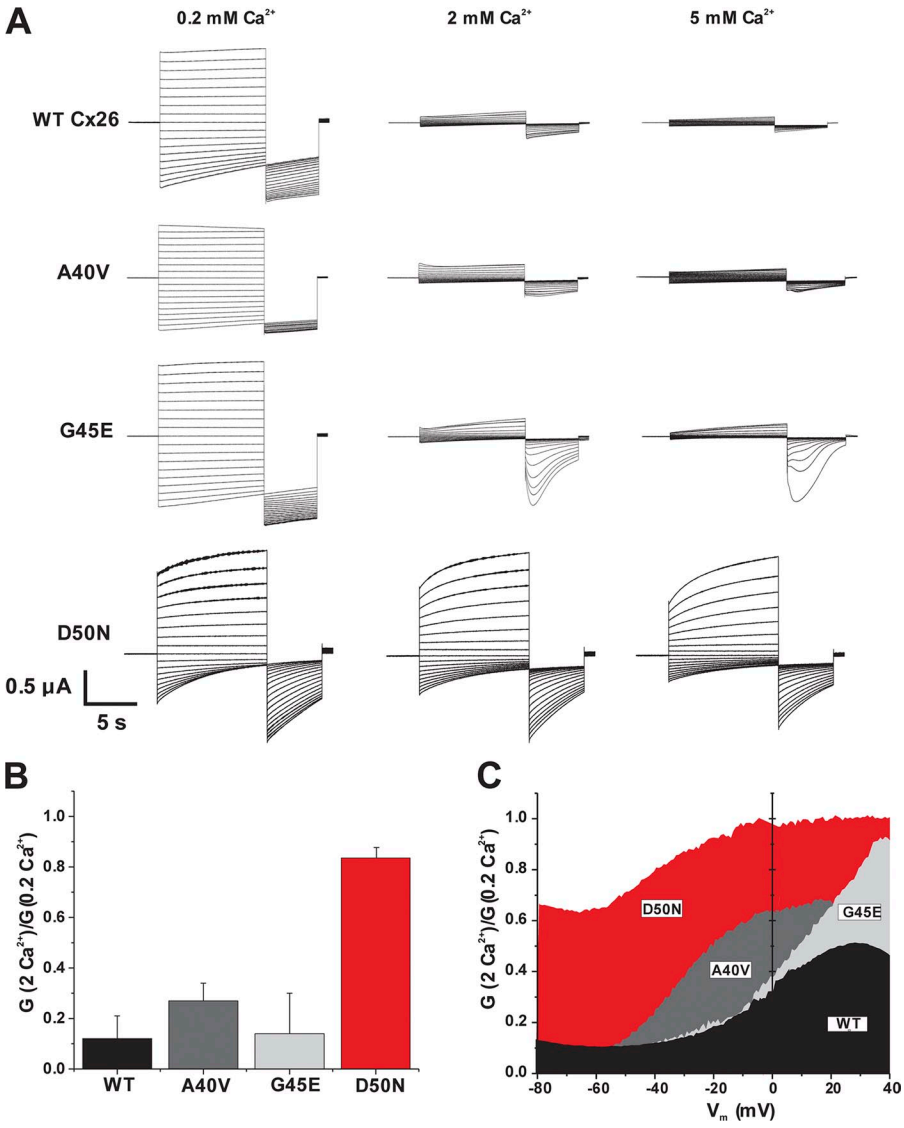

Figure 1. The D50N KID mutation exhibits substantially impaired regulation by extracellular Ca^{2+} over a wide voltage range. (A) Representative hemichannel currents in *Xenopus* oocytes obtained using a voltage step protocol that consisted of 10-s steps, from 60 to −110 mV in intervals of 10 mV, followed by a 5-s step to −110 mV. Oocytes were voltage clamped to −20 mV between steps. Currents shown in each case are from single oocytes exposed to all three Ca^{2+} concentrations. WT Cx26, A40V, and G45E all showed substantial reductions in current magnitude at the higher Ca^{2+} concentrations, whereas D50N was nearly insensitive. (B) Bar graph showing ratios of the values of the macroscopic conductances measured in 2 and 0.2 mM Ca^{2+}, $G_{2Ca^{2+}}/G_{0.2Ca^{2+}}$. The conductances were calculated from currents elicited by brief (1 s) voltage steps of ±10 and 20 mV from a holding potential of −20 mV. D50N exhibits near insensitivity to Ca^{2+}. Each bar represents the mean ratio ± SE. n = 12 for WT Cx26, 8 for A40V, 12 for G45E, and 10 for D50N. (C) Plots showing mean ratios of macroscopic conductances measured in 2 and 0.2 mM Ca^{2+}, $G_{2Ca^{2+}}/G_{0.2Ca^{2+}}$, over a voltage range of −80 to 40 mV. G-V curves were obtained from voltage ramps applied from 40 to −100 mV, 600 s in duration. Oocytes were held at a holding potential of −20 mV. Before initiating the ramps, oocytes were stepped to 40 mV for 30 s to allow conductance to reach steady-state. Ca^{2+} regulation shows some voltage dependence, with more effective inhibition of currents at large negative membrane potentials. D50N shows poor Ca^{2+} regulation over the entire voltage range.

in other connexins (Kronengold et al., 2003; Verselis, 2009; Verselis et al., 2009).

SCAM confirms that D50 is a pore residue in Cx26 hemichannels

To assess whether D50 is exposed to the pore lumen in Cx26 hemichannels, we made a D50C substitution and examined accessibility of the Cys side chain to thiol-specific MTS reagents. D50C hemichannels were functional, and application of the oppositely charged reagents, MTSET and MTSES, altered D50C currents in opposite ways. MTSET reduced current magnitude, whereas MTSES increased it (Fig. 3, A and B). In both cases, the changes in current occurred rapidly (within seconds), did not reverse upon washout, and were refractory to a second addition of MTS reagent. Mean changes in current compiled from several experiments are plotted in Fig. 3 C for MTSET, MTSES, and the larger MTS biotin-X reagent. No effects of MTS reagents were observed for WT Cx26 or D50N hemichannels (not depicted).

At the single hemichannel level, we found that modification by MTS reagents strongly altered unitary conductance and open state rectification. Shown in Fig. 3 (D–F) are examples of unitary D50C currents in response to ±70-mV voltage ramps recorded from cell-attached patches. Unitary conductance and open hemichannel rectification of D50C hemichannels was similar to D50N hemichannels (Fig. 3 D). After exposure to MTSES, D50C hemichannel properties changed, exhibiting a unitary conductance and open hemichannel current rectification similar to WT Cx26 (Fig. 3 E). After exposure to MTSET, unitary conductance became even smaller than D50C and outward current rectification remained strong (Fig. 3 F). The same effects of MTS modification were observed when reagent was added to the extracellular or cytoplasmic sides of hemichannels in outside-out and inside-out patch configurations, respectively. These results indicate that the D50C side chains are readily modified by MTS reagents and that modification significantly impacts ionic conduction consistent with exposure of this residue to the aqueous pore in open Cx26 hemichannels.

D50N and voltage gating

Closure of Cx hemichannels with membrane hyperpolarization is mediated by a form of voltage-dependent gating, termed loop or slow gating (Trexler et al., 1996; Bukauskas and Verselis, 2004). At the single channel level, loop gating is characterized by gating transitions between open and fully closed states that appear slow as the result of transit through a series of transient substates (Trexler et al., 1996). Another form of gating, termed V_j or fast gating, closes hemichannels to a substate, and for Cx26 hemichannels this occurs at relatively large positive membrane voltages (Sánchez et al., 2010). Extracellular Ca^{2+} selectively modulates loop gating and serves to limit hemichannel opening, in large part, by shifting activation of loop gating substantially positive (Verselis and Srinivas, 2008).

Normalized G-V relationships for WT Cx26 hemichannels are illustrated in Fig. 4 A at two extracellular Ca^{2+} concentrations differing 10-fold in concentration, 0.2 and 2 mM. We focused on voltages between −100 and 40 mV, where loop gating occurs with minimal interference from V_j or fast gating. For WT Cx26, activation of loop gating in 0.2 mM Ca^{2+} occurred at large negative voltages and shifted robustly positive, ∼50 mV, in 2 mM Ca^{2+}; maximal conductance also decreased. For D50N hemichannels, loop gating remained strong but, as previously shown in Fig. 1, was largely insensitive to the extracellular Ca^{2+} concentration (Fig. 4 B). Moreover, activation was shifted to a voltage intermediate between 0.2 and 2 mM Ca^{2+} for WT Cx26 (Fig. 4 C). These data suggest that the D50N mutation does not simply inhibit Ca^{2+} binding, which would have fixed activation at large negative voltages comparable with that for WT Cx26 in the absence of added Ca^{2+}. Thus, the D50N mutation appears to substantially alter the chemical free energy difference between the open and closed states mediated by loop gating, resulting in a shift in activation.

Recordings at the single hemichannel level confirm that the D50N mutation affects loop gating (Fig. 5). Shown are cell-attached patch recordings of D50N hemichannels with EGTA in the pipette to maintain a

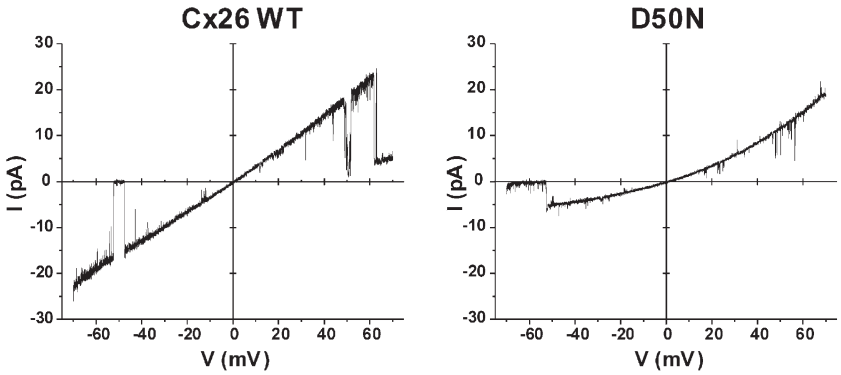

Figure 2. The D50N mutation substantially alters open-state conductance and rectification of Cx26 hemichannels. Representative examples of patch-clamp recordings from inside-out patches containing single WT Cx26 (left) and D50N (right) hemichannels are shown. Currents shown were obtained in response to 8-s voltage ramps applied between ±70 mV and leak subtracted (see Materials and methods). WT Cx26 shows slight outward rectification, whereas D50N exhibits a reduced slope conductance (measured at 0 mV) and strong outward rectification. Bath and pipette solutions consisted of IPS (see Materials and methods).

submicromolar Ca^{2+} concentration. A patch containing several D50N hemichannels shows gating events almost exclusively between open and fully closed states with transitions that typify loop gating (Fig. 5, see inset at 40 mV). Histograms to the left of each recording from −20 and 40 mV show equally spaced peaks representing full open/closed transitions. At 50 mV, gating to substates becomes very evident, which is ascribable to the onset of V_j or fast gating. The significantly reduced opening of D50N hemichannels at −20 mV is consistent with the strong positive shift in activation observed in macroscopic recordings in low extracellular Ca^{2+}. Examples of recordings of WT Cx26 at two voltages, −30 and 30 mV, are shown for comparison. The gating transitions are all loop gating transitions as well, but the open probabilities are similar at −30 and 30 mV, consistent with the more negatively shifted activation of loop gating for WT Cx26 in low extracellular Ca^{2+}. An interesting characteristic of Cx26 and D50N hemichannels is that gating remains active at all voltages. This behavior

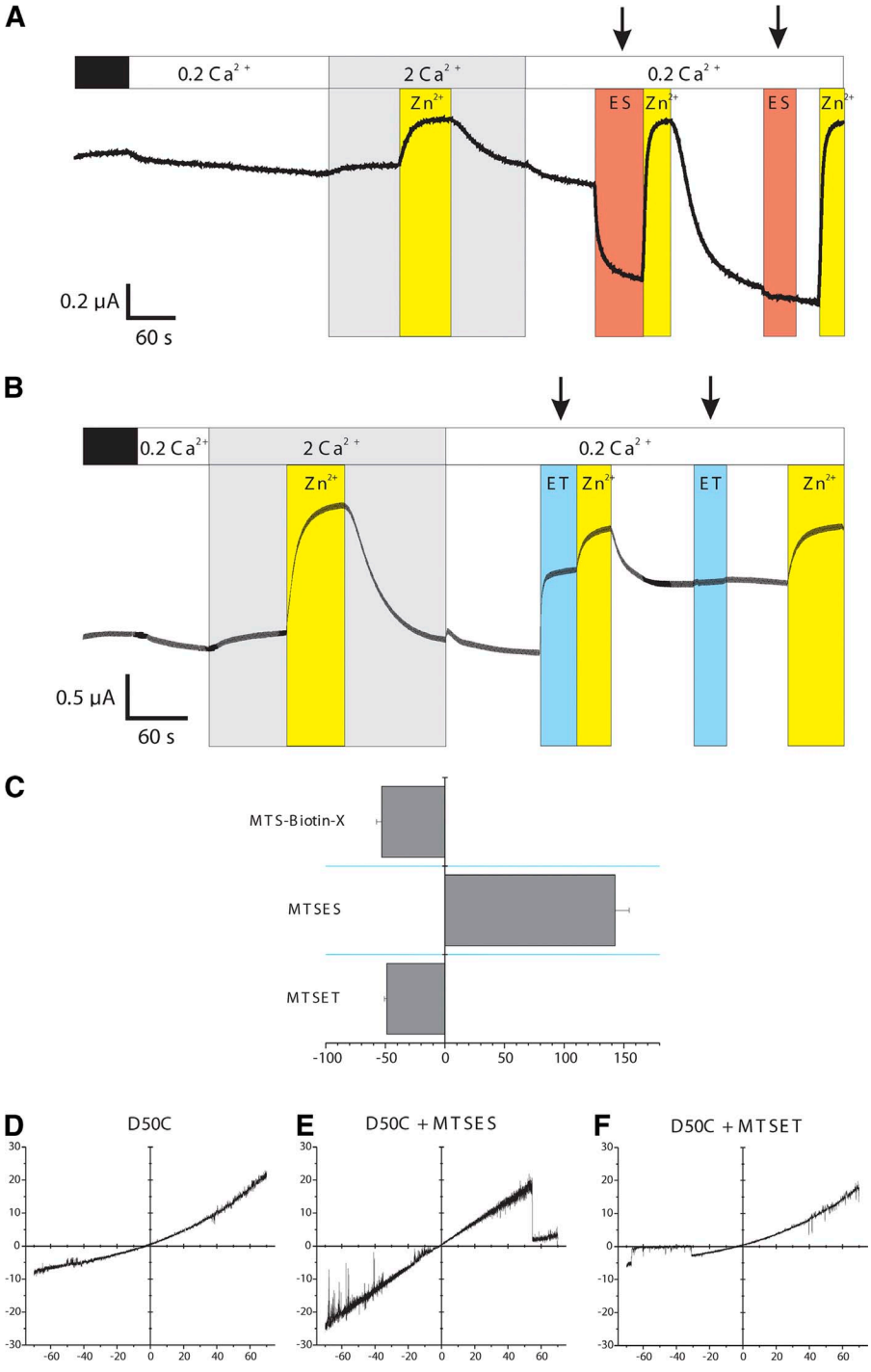

Figure 3. SCAM experiments using MTS reagents indicate D50 is a pore-lining residue. (A and B) Shown are effects of MTSES (A) and MTSET (B) on macroscopic D50C hemichannel currents. Oocytes were held at −40 mV throughout. Oocytes were exposed to 100 mM NaCl salt solutions with Ca^{2+} concentrations as indicated in the top bar; black segments indicate oocytes were initially bathed in MND96. Because of the poor sensitivity to Ca^{2+}, 200 µM Zn^{2+} (yellow segments) was used to periodically close D50C hemichannels. Application of 2 mM MTSES and 0.2 mM MTSET is indicated by arrows above the orange and blue segments, respectively. (C) Summary of the percent change in current (mean ± SE) after application of each reagent. n = 43 for MTSES, 18 for MTSET, and 4 for MTS-biotin X. (D–F) Representative examples of patch-clamp recordings obtained from cell-attached patches containing single D50C hemichannels recorded from oocytes that were not exposed to MTS reagents (D), were exposed to 2 mM MTSES (E), and were exposed to 0.2 mM MTSET (F). All unitary currents were obtained in response to 8-s voltage ramps between ±70 mV and leak subtracted. Bath and pipette solutions consisted of IPS.

contrasts that of Cx46 and Cx50 hemichannels, in which open probabilities approach unity in this voltage range under low Ca^{2+} conditions (Srinivas et al., 2005; Verselis and Srinivas, 2008; Rubinos et al., 2012).

Effects of substitutions at position 50: Unitary hemichannel properties and Ca^{2+} regulation

Fig. 6 (A and B) compares the effects on unitary conductance and open hemichannel rectification for several D50 substitutions, including D50N, D50A, D50E, and D50C, as well as D50C modified by MTS reagents. D50A and D50C hemichannels resembled D50N. When D50C hemichannels were modified by MTSET, they remained strongly outwardly rectifying, with unitary conductance reduced even more than D50N. Conversely, modification of D50C hemichannels by MTSES largely restored open hemichannel conductance and rectification to WT Cx26 values. Likewise, when we made the D50E conservative charge substitution, open hemichannel properties resembled WT Cx26. Thus, open hemichannel properties resembled WT when we placed a negative charge at position 50, with considerable flexibility regarding the specific chemical nature of the charged moiety.

For Ca^{2+} regulation (Fig. 6, C and D), D50A behaved much like D50N. D50C exhibited an intermediate level of inhibition between WT Cx26 and D50A or D50N. D50E, a conservative charge substitution, largely restored Ca^{2+} regulation at negative voltages but not as robustly at positive voltages. Modification of D50C hemichannels by MTSES, which also places a negative charge at position 50, was difficult to quantify because exposure to high Ca^{2+} after modification led to a variable degree of rundown. In the few examples that showed modest rundown, there was stronger regulation by Ca^{2+}, but it did not resemble that of WT hemichannels. D50C hemichannels modified by MTSET remained largely insensitive to Ca^{2+} over the entire voltage range. Thus, unlike unitary conductance and open state rectification, recapitulation of WT-like sensitivity to Ca^{2+} was not achieved by simply placing a negative charge at position 50. These data indicate that the presence of a negative charge at this position creates a condition favorable for the actions of Ca^{2+}, although Asp appears to be optimal.

D50 and intersubunit interactions

The crystal structure of the Cx26 GJ channel suggests that D50 may participate in intersubunit interactions (Maeda et al., 2009). One possible interacting residue is K61 in the E1 domain, which in the published structure was shown to interact with the main chain carbonyl of TM1 at Phe^{51} (Fig. 7 B, 2ZW3). However, analysis of an electron density map calculated with coefficients of structure factors deposited in the Protein Data Bank (2zw3sf.mtz file; Protein Data Bank accession no. 2ZW3) suggests an alternative structure in which K61 and D50 from adjacent subunits interact making for a possible D50–K61 salt bridge (Fig. 7 B, 2ZW3rev). Both structures are interconvertible to each other by rotation around the CD-CE single bond without any short nonbonding contact. Moving down the pore from D50 toward the cytoplasm, the next putative pore residue in the structure is D46. Both D50 and D46 are positioned

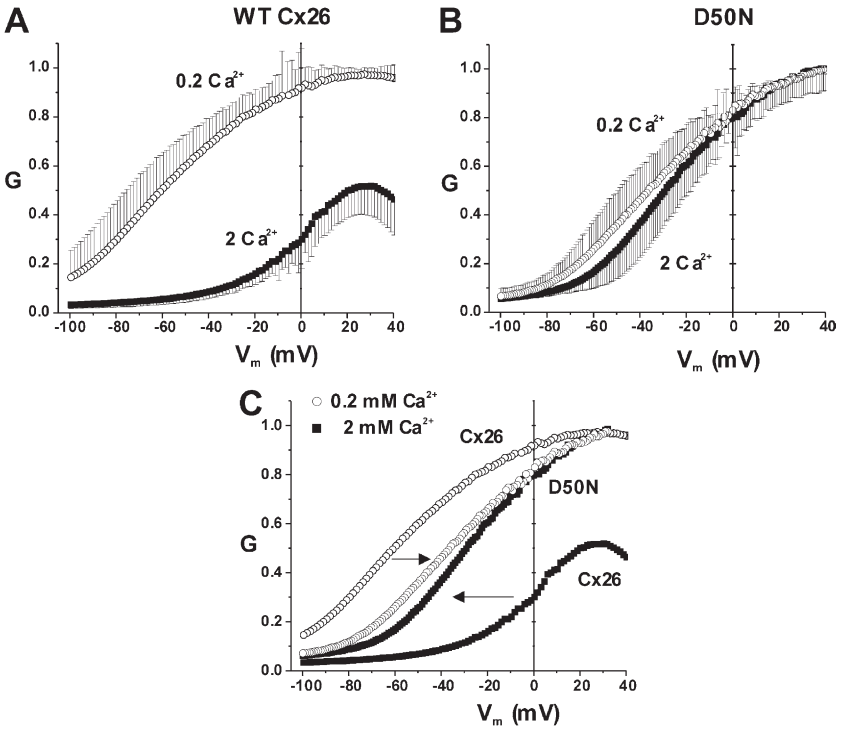

Figure 4. Loop gating remains strong in D50N, but activation is shifted compared with WT Cx26. (A and B) Shown are normalized G-V relationships of WT Cx26 (A) and D50N (B) hemichannels expressed in *Xenopus* oocytes at two different external Ca^{2+} concentrations, 0.2 and 2 mM. Data were obtained by applying slow (600 s) voltage ramps from 40 to −100 mV from a holding potential of −20 mV. Ramps were obtained for each oocyte in 0.2 and 2 mM Ca^{2+} and normalized to the maximum value measured in 0.2 mM Ca^{2+}. In WT Cx26, increasing Ca^{2+} shifted activation in the depolarizing direction and suppressed current magnitude. D50N was nearly insensitive to Ca^{2+}. Each symbol represents the mean value. n = 11 for WT Cx26 and 7 for D50N. For clarity, only error bars for +SE are shown for 0.2 mM Ca^{2+} and −SE for 2 mM Ca^{2+}. (C) Superimposition of G-V curves for WT and D50N with error bars omitted for clarity. Compared with WT Cx26, activation of D50N is shifted positive in low Ca^{2+} (0.2 mM) conditions and negative in high Ca^{2+} conditions (2 mM). Data are the same as in A and B.

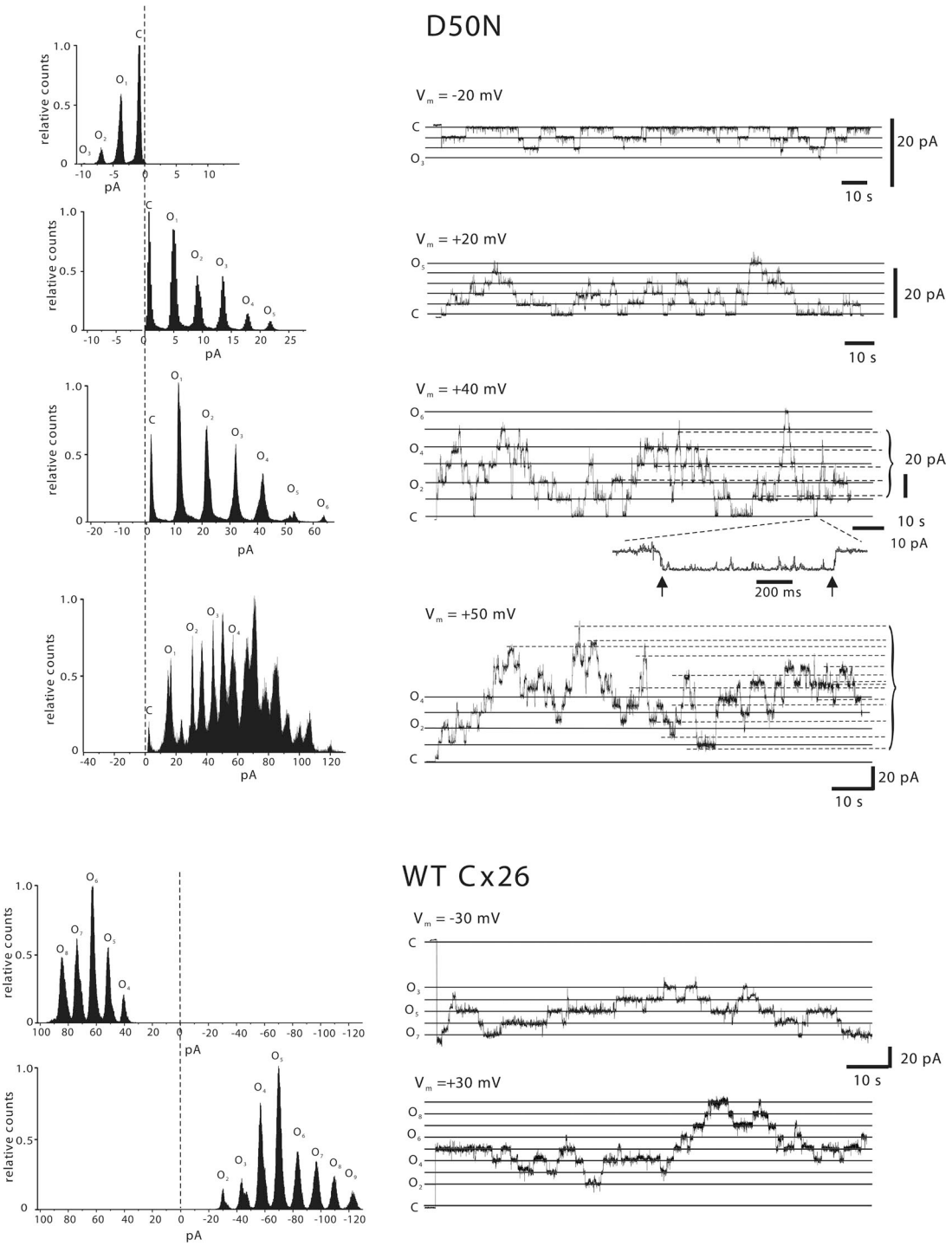

Figure 5. Single hemichannel recordings demonstrate that D50N affects loop gating. Multichannel cell-attached patch recordings of D50N and Cx26 WT hemichannels are shown. The patch pipette and bath solutions consisted of IPS. For the D50N, shown are 2–3-min consecutive segments of current recorded at membrane potentials of −20, 20, 40, and 50 mV. The solid lines designated *C* represent the leak conductance of the patch when no hemichannels were open. Solid lines designated O_n represent current levels of single or multiple fully open hemichannels. Dashed lines represent intermediate conductances (substates). All point histograms obtained from these recordings are shown to the left of each trace. At voltages of −20, 20, and 40 mV, gating events are uniform in size and represent transitions between closed and fully open hemichannels. The inset below the 40 mV trace shows an open and closing transition at an expanded time scale that is characteristic of loop gating. At 50 mV, many subconducting transitions become evident and are consistent with the onset of V_j or fast gating. Note that D50N hemichannels exhibit substantial closure even at −20 mV as expected because of the shift in loop gating caused by the mutation. For the Cx26 WT hemichannel, the currents shown were recorded at −30 mV and 30 mV. Note that open probability for WT Cx26 is similar at both voltages. All currents were filtered at 1 kHz, and data were acquired at 5 kHz.

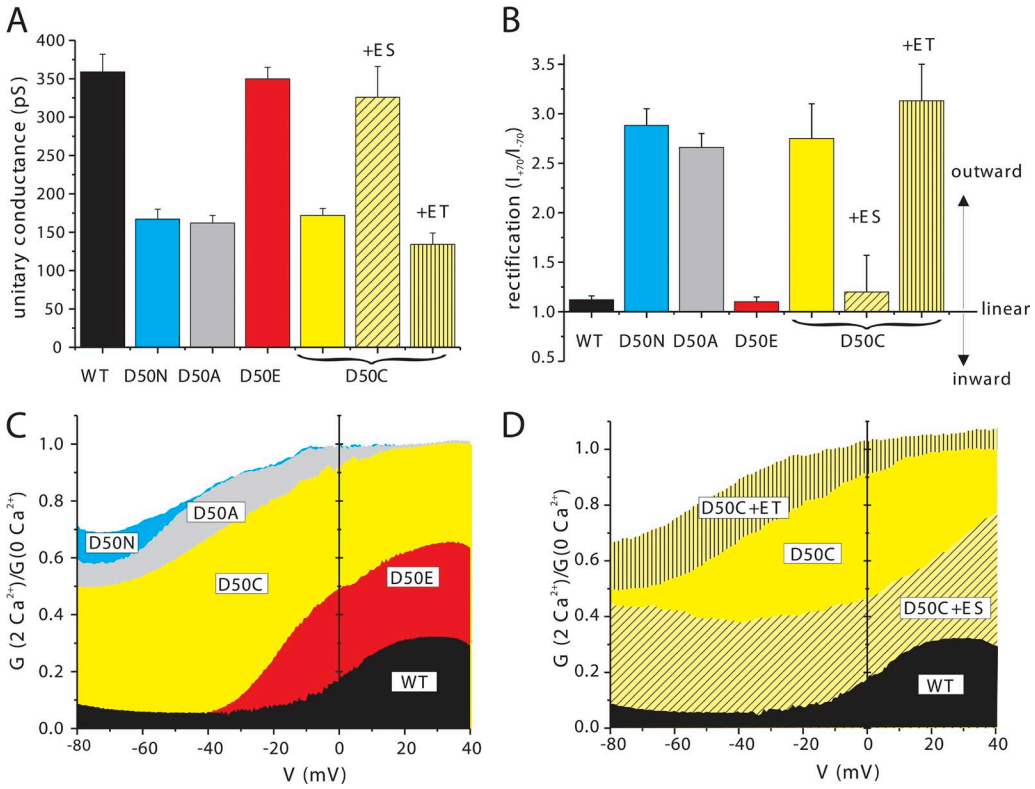

Figure 6. The presence of a negative charge at position 50 confers WT open hemichannel properties but a variable degree of Ca^{2+} regulation. (A and B) Values of unitary conductance (A) and open hemichannel rectification (B) for WT Cx26 and several D50 mutant hemichannels. Each bar represents the mean value ± SD; n = 18 for WT Cx26, 16 for D50N, 14 for D50A, 10 for D50E, 11 for D50C, 8 for D50C + MTSES, and 12 for D50C + MTSET. Open hemichannel conductance was measured as the slope conductance at V_m = 0. Rectification was measured as the ratio of the open hemichannel current at 70 and −70 mV. (C and D) Plots showing mean ratios of the macroscopic conductances measured in 2 and 0.2 mM Ca^{2+}, $G_{2Ca^{2+}}/G_{0.2Ca^{2+}}$ over a voltage range of −80 to 40 mV. G-V curves were obtained from slow voltage ramps as described in Fig. 1 C. (C) Plots superimposing WT Cx26 and mutants with different substitutions at position 50. (D) Plots superimposing WT Cx26 and the D50C mutant, unmodified and modified with MTSET or MTSES.

to potentially interact via hydrogen bonding with Q48 from the adjacent subunit. D46 also can potentially form an intrasubunit salt bridge with R184 (an E2 residue), which can potentially form an intersubunit salt bridge with D47. To test the two putative intersubunit interactions directly involving D50, K61–D50 and Q48–D50, we mutated each position to Ala, individually and in paired combinations. Ala substitution was used to avoid possibilities for side chain interactions.

For K61, substitution to Ala resulted in loss of hemichannel function. K61C also failed to function. However, K61 mutants coexpressed with WT Cx26 or D50N produced functional hemichannels. When coexpressed with D50N, the hemichannel currents exhibited Ca^{2+} sensitivity. Fig. 8 A compares Ca^{2+} regulation in homomeric D50N and WT Cx26 hemichannels with those formed from a D50N:K61C mixture of injected mRNAs at a ratio of a 1:4 to bias expression toward K61C. Plotted are conductance ratios in 2 and 0.2 mM Ca^{2+}. Stronger inhibition by Ca^{2+} was clearly evident and intermediate between D50N and WT Cx26, indicating that mutation of K61, unlike D50, does not interfere with Ca^{2+} regulation. Patch recordings on these same cells exhibited single hemichannels with conductance and rectification intermediate between D50N and WT Cx26. Examples of single hemichannel currents (ramps) obtained from different patches on the same oocyte are shown in Fig. 8 B. The currents either resembled D50N or appeared somewhat larger and less outwardly rectifying. Data from several patches is summarized in Fig. 8 C. Application of MTSET or MTSES (Fig. 8 C, open symbols) did not affect the unitary currents of these hemichannels. Although not shown, coexpressing K61C with WT Cx26 resulted in unitary conductances indistinguishable from WT Cx26. Overall, these results suggest K61 is not freely exposed to the pore lumen, in disagreement with the Cx26 crystal structure. Also, K61C/A subunits possess essentially WT properties, inconsistent with a simple role for K61 as an interacting partner with D50, in which mutation of K61 would be expected to produce an equivalent phenotype as mutation of D50 via disruption of a D50–K61 interaction.

For Q48, substitution to Ala yielded functional hemichannels. The Q48A + D50A double mutant also

functioned. Shown in Fig. 9 A are mean normalized G-V curves for WT, Q48A, D50A, and Q48A + D50A hemichannels in 0 (nominal) and 2 mM Ca^{2+}. As previously indicated, D50A resembles D50N, being nearly insensitive to extracellular Ca^{2+} with activation shifted to an intermediate value between that of WT Cx26 in 0 and 2 mM Ca^{2+}. Q48A also exhibited a positive shift in activation in low Ca^{2+} but continued to shift robustly positive in 2 mM Ca^{2+}. The double mutant, Q48A + D50A, resembled D50A alone, although activation was shifted somewhat more positive.

To assess whether there was evidence of an interaction between Q48 and D50, we applied mutant cycle analysis to the voltage dependence of loop gating. To extract gating parameters separate from open hemichannel rectification, we used a stochastic gating model developed for GJ channels (Paulauskas et al., 2009, 2012) and adapted it to hemichannels (see Materials and methods). Fig. 9 B shows the G-V relations derived from the obtained gating parameters, each individually normalized to maximum conductance. For both Ca^{2+} conditions, the gating parameters, z (apparent gating charge) and $V_{1/2}$ (voltage for half-maximal activation), are provided in Table 1 along with the calculated free energy differences (ΔG^0s) between open and closed states and the calculated Q48A–D50A coupling energy, $\Delta G_{coupling}$. In 0 mM Ca^{2+}, the shift in $V_{1/2}$ for the double Q48A + D50A mutant was similar to D50A alone, yielding a modest coupling energy of ~0.7 kcal/mol. In 2 mM Ca^{2+}, the G-V relationships yielded a weaker coupling energy of ~0.2 kcal/mol. The stronger coupling energy in the absence of Ca^{2+} suggests that D50 and Q48 preferentially interact in the absence of Ca^{2+} and that Ca^{2+} may serve to weaken or disrupt this interaction and to shift hemichannel activation positive.

Because of the potentially complex network of interactions present in the TM1/E1 region (Fig. 7), the Q48–D50 coupling energy we measured may have been the result of indirect interactions via structural alterations in this region of the hemichannel. To investigate

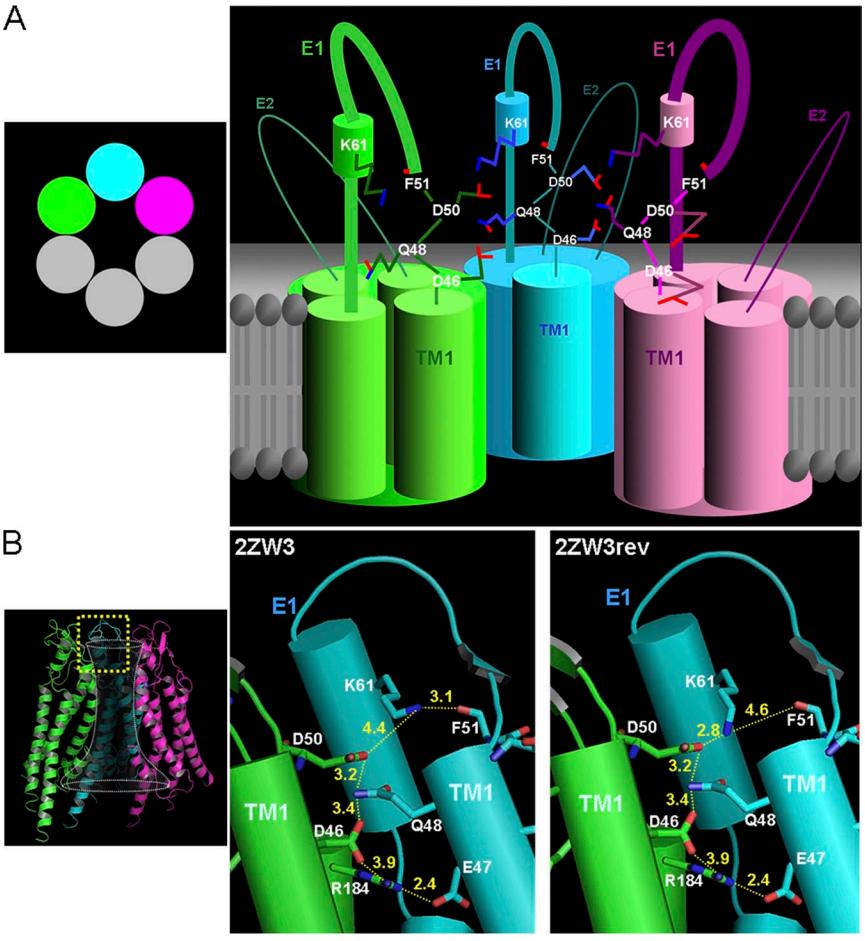

Figure 7. Possible intra- and intersubunit interactions at the border of TM1 and E1 of Cx26. (A) Illustration depicting three of six connexin subunits around a central aqueous pore. Each subunit is represented by a different color. Cylinders inside the subunits represent the transmembrane domains. TM1 denotes the first transmembrane domain that is exposed to the pore. E1 and E2 denote the first and second extracellular loop domains, respectively. D50 and D46 residues in E1 of each subunit are shown projecting into the pore. For the green (left) and cyan (middle) subunits, the D50 side chains come into proximity with K61 (situated on a short helix in E1) and Q48 (in E1) from the adjacent subunits. D46 also comes into close proximity to Q48. The illustration is not drawn to scale or strictly according to the atomic structure to emphasize the arrangement of interacting residues at the extracellular end of the pore. (B) Representation of the same three connexin subunits that constitute a Cx26 hemichannel viewed from the pore using the atomic structure published by Maeda et al. (2009). The superimposed cone in the left panel depicts the gross shape of the pore. The boxed region is shown in two expanded views to highlight the interacting residues between the green and cyan subunits. Only segments A39-R75 and C180-E187 are displayed in the expanded views for clarity. In the originally published structure (Protein Data Bank accession no. 2ZW3; middle), K61 in the cyan subunit is shown in close proximity to the backbone carbonyl of F51 in the same subunit. D50 and Q46 in the green subunit are in close proximity to Q48 from the adjacent (cyan) subunit. Other putative interactions shown are D46 with R184 in the same (green) subunit and R184 with D47 of next adjacent (cyan) subunit. Segments of E1 and TM1 are indicated. In the alternative structure (2ZW3rev; right) K61 in the cyan subunit is positioned in closer proximity to D50 in the adjacent (green) subunit. Structures were generated using PyMOL software.

the possibility of a direct Q48–D50 intersubunit interaction, we constructed individual Cys mutants, D50C and Q48C, as well as a double-Cys mutant, Q48C + D50C, and examined whether there was evidence for intersubunit disulfide bond formation, both functionally and biochemically. Functionally, we did not observe hemichannel currents in oocytes injected with Q48C + D50C, but currents did develop upon addition of 1–2 mM DTT to the bath. This DTT dependence suggested that Q48C and D50C may have formed a disulfide bond that impaired hemichannel opening. However, the single Q48C mutant hemichannel also required DTT to function. Examples of recordings are shown in Fig. 10. For both single Q48C and double Q48C + D50C mutants, no currents developed upon exposure to low Ca^{2+} alone but developed when DTT was added. Q48C + D50C hemichannels differed in that currents developed more slowly and usually to lower levels compared with Q48C hemichannels. Also, Q48C + D50C currents remained the same after washout of DTT, whereas the Q48C currents declined fairly rapidly back to baseline after washout, consistent with rapid disulfide reformation. This difference in kinetics and reversibility suggests that the nature of the disulfide bonds and/or their local environments differ in the single and double mutants. The DTT dependence of both of these mutants contrasted with that of D50C, which functioned well without DTT and exhibited only a small increase in current upon exposure to 1–2 mM DTT that did not reverse upon washout. WT Cx26 hemichannels were unaffected by exposure to 1–2 mM DTT as were Q48A mutants (recordings not depicted); the latter rules out a general structural rearrangement with any Q48 substitution that leads to DTT dependence caused by inappropriate disulfide formation involving only endogenous Cys residues. Data summarizing effects of DTT on hemichannel function are shown in Fig. 10 B. TPEN, a metal chelator, was also tested but had no effect (not depicted), ruling out metal bridges as a cause of the functional effects (Tang et al., 2009; Verselis et al., 2009).

To examine biochemical evidence for disulfide bond formation, we ran Western blots of protein extracted from oocytes expressing WT Cx26, D50C, Q48C, and Q48C + D50C under nonreducing (−DTT, −ME) and reducing (+DTT, +ME) conditions (Fig. 11). WT Cx26 shows only a monomer band at ∼25 kD with and without reducing conditions. However, D50C, Q48C, and Q48C + D50C all showed evidence of intersubunit disulfide bond formation. In nonreducing conditions, both Q48C and D50C exhibited a prominent higher molecular mass band (∼40 kD) consistent with dimer formation.

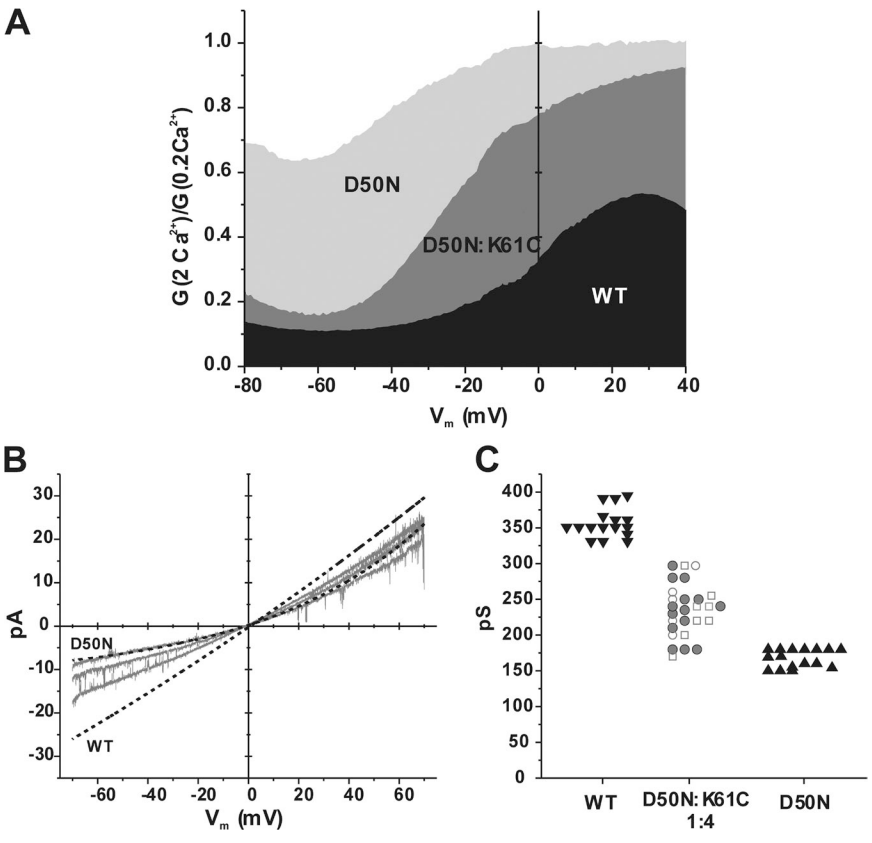

Figure 8. K61C functions as a heteromer and confers Ca^{2+} regulation. (A) Plots showing mean ratios of the macroscopic conductances measured in 2 and 0.2 mM Ca^{2+}, $G_{2Ca}{}^{2+}/G_{0.2Ca}{}^{2+}$, over voltage range from −80 and 40 mV. G-V curves were obtained in oocytes injected with mRNA for WT Cx26, D50N mutant, and a 1:4 mixture of D50N:K61C. Oocytes injected with K61C alone did not exhibit measureable currents (not depicted). (B) Examples of single hemichannel currents obtained from an oocyte expressing D50N:K61C in a 1:4 ratio (gray lines). Currents are in response to voltage ramps applied from 70 to −70 mV. Each trace represents a separate patch with selected examples of hemichannels with intermediate conductance and rectification properties. Representative I-V relations of open WT Cx26 and D50N hemichannels are displayed as dashed lines. (C) Values of unitary hemichannel conductance measured as the slope conductance at V_m = 0 for WT Cx26 (▼), D50N:K61C (gray circles), and D50N (▲). Values for D50N:K61C include those after exposure to MTSET (□) or MTSES (○). Each point represents data from a separate patch. WT Cx26 and D50N hemichannels each clustered tightly about their mean values, whereas D50N:K61C was spread out over a wider range, indicative of hemichannels with different conductances.

However, the double Q48C + D50C mutant showed this band and additional high-molecular weight bands consistent with multimer formation. In all cases, inclusion of DTT + ME resulted in monomer bands only. Thus, individual Q48C and D50C substitutions appear to be capable of forming disulfides resulting in dimers. These results suggest Q48C can interact with Q48C in pairs across subunits. The same is true for D50C. For the Q48C + D50C double mutant, multimer formation is consistent with interaction across subunits as the result of the availability of disulfides that can link all subunits.

Effects of substitutions on GJ channels

Because the TM1/E1 region, and consequently the potential interactions in this region, may be altered upon docking of the extracellular loops, we examined the impact of substitutions at Q48, D50, and K61 on GJ channel function. The data are summarized in Table 2. The D50N mutation, as previously reported by Lee et al. (2009), shows no evidence of GJ channel function despite robust hemichannel function. We confirmed this and observed the same for D50A and D50C in paired oocytes and transfected N2A cells. Conversely, K61A and K61C mutants, which did not function as hemichannels, functioned as GJ channels with unitary conductances ~30–40% higher than WT Cx26. Q48A, which functioned as a hemichannel, also functioned as a GJ channel. Q48C, which functioned as a hemichannel only in the presence of DTT, functioned as a GJ channel without DTT. The unitary conductances of these Q48 mutants were essentially the same as WT Cx26. The double Q48A + D50A and Q48C + D50C mutants exhibited low levels of coupling between N2A cells, suggesting mutation of Q48 has an effect on D50

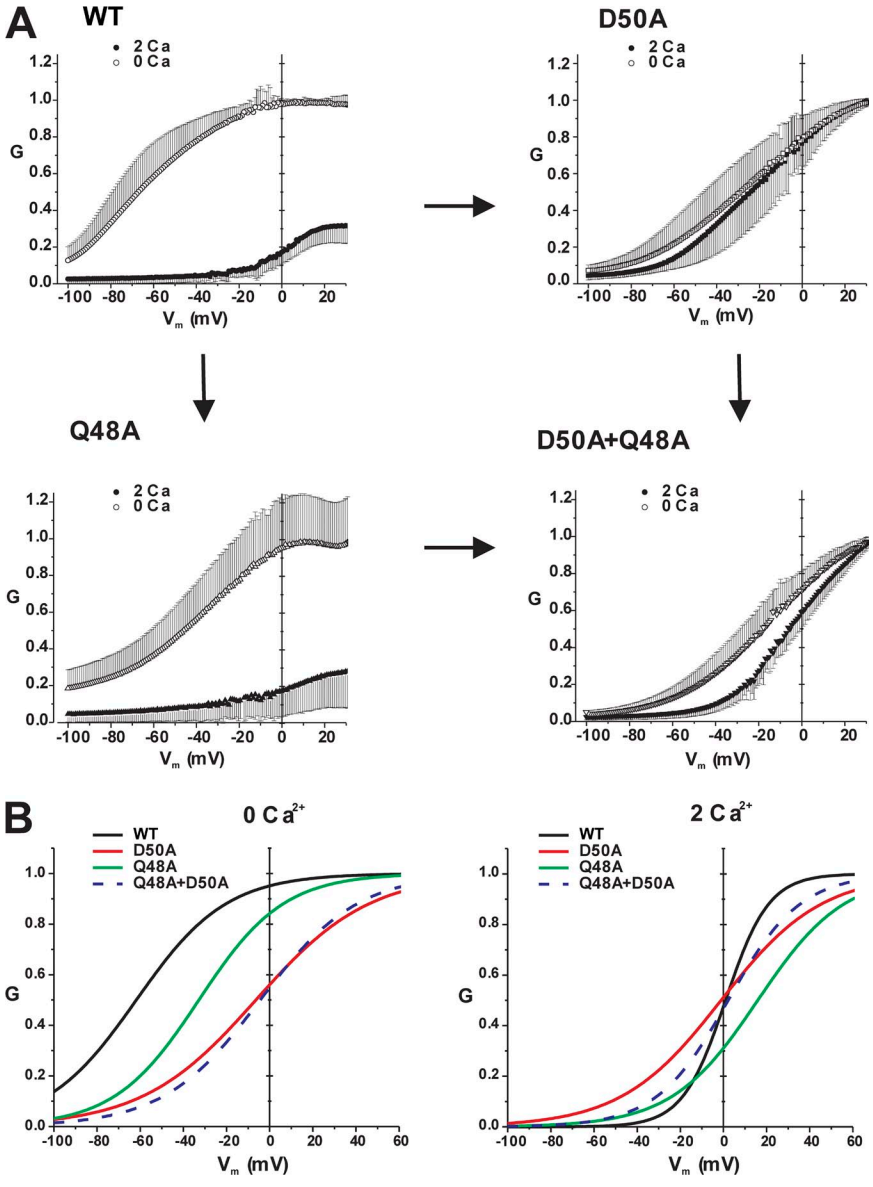

Figure 9. Mutant cycle analysis suggests that D50 and Q48 residues interact. (A) G-V relationships for WT Cx26, D50A, Q48A, and double mutant D50A + Q48A hemichannels at two different external Ca^{2+} concentrations, 0 (or nominal) and 2 mM. Data were obtained by applying slow (600 s) voltage ramps from 40 to −100 mV from a holding potential of −20 mV. For each oocyte, conductances at both Ca^{2+} concentrations were normalized to the maximum value in 0 mM Ca^{2+}. $n = 11$ for WT Cx26, 17 for D50A, 14 for Q48A, and 6 for D50A + Q48A. The G-V curves are arranged as a mutant cycle where residues D50 and Q48 are mutated separately and together. The arrows connecting each pair of hemichannel phenotypes refer to mutation of either the D50 residue (horizontal arrows) or the Q48 residue (vertical arrows). The double D50A + Q48A mutant resembles D50A alone, suggestive of an interaction between D50 and Q48. (B) Fitted G-V_m relations normalized to their maximum conductance obtained by fitting data to a stochastic gating model developed for connexin channels (Paulauskas et al., 2009, 2012; see Materials and methods). These G-V curves represent voltage-dependent gating independent of rectification of open hemichannels. G-V curves for WT and mutant hemichannels are superimposed in 0 mM Ca^{2+} (left) and 2 mM Ca^{2+}. Note the similarity of phenotypes displayed by D50A and double mutant D50A + Q48A in 0 and 2 mM Ca^{2+}.

mutations in terms of GJ channel function. Thus, mutations in the TM1/E1 region have different effects in hemichannels and GJ channels, suggesting there may be some structural rearrangements in this region upon docking that affect how substitutions at certain positions influence subunit interactions and impact function.

DISCUSSION

In this study, we find that D50N, the most common Cx26 mutation in *GJB2* associated with KID syndrome, produces multiple effects on Cx26 channel function. In hemichannels, D50N resulted in a loss of inhibition by extracellular Ca^{2+}, shifted voltage-dependent loop gating, reduced unitary conductance, and increased outward rectification of single open hemichannel current. For GJ channels, D50N results in loss of function, as previously reported (Lee et al., 2009), and we find that this loss of function extends to several other substitutions at this position.

Confirmation of D50 as a pore-lining residue explains the altered single open hemichannel properties of the D50N mutation

Our SCAM and mutational experiments indicate that D50 is a pore-lining residue in Cx26 hemichannels. Both from the single hemichannel properties exhibited by various D50 substitutions and by the D50C substitution modified by MTS reagents, the altered conductance and rectification characteristic of D50N hemichannels can be explained by the removal of a ring of negative charge, normally contributed by D50, at the extracellular end of the pore. Ala and Cys substitutions, as well as Cys modified by MTSET all behaved similar to D50N, whereas a Glu substitution or a Cys substitution modified by MTSES behaved like WT Cx26. These data indicate that the dominant factor responsible for conferring WT open hemichannel conductance and rectification at this position is the presence of a negative charge, whether it is an Asp, Glu, or an unnatural sulfonate resulting from MTSES modification of Cys. Such a general electrostatic role for a pore-lining residue is plausible in a large aqueous pore where ionic flux does not involve complete or partial dehydration of ions and coordination with specific residues. Residence of D50 in the pore is consistent with the crystal structure of the Cx26 GJ channel and with SCAM studies of Cx46 and Cx50 hemichannels that showed the homologous position, D51, is exposed to the pore in the open state (Kronengold et al., 2003; Verselis et al., 2009).

TABLE 1

Activation and coupling energies of Cx26 WT, Q48A, D50A, and Q48A + D50A hemichannels

Cx26	z	$V_{1/2}$	ΔG^0	$\Delta(\Delta G^0)$	$\Delta G^0_{coupling}$
		mV	*kcal/mol*		
WT					
(0 mM Ca^{2+})	1.2	−61.8	−1.65		
(2 mM Ca^{2+})	2.8	1.0	0.07		
Q48A					
(0 mM Ca^{2+})	1.3	−32.8	−0.95	0.70	
(2 mM Ca^{2+})	1.0	15.9	0.34	−0.27	
D50A					
(0 mM Ca^{2+})	0.9	−6.4	−0.14	1.51	
(2 mM Ca^{2+})	1.1	−1.1	−0.03	0.10	
Q48A + D50A					
(0 mM Ca^{2+})	1.1	−4.4	−0.11	1.54	0.67
(2 mM Ca^{2+})	1.5	2.2	0.08	0.01	0.17

Empty cells indicate that the information is not applicable.

D50N and hemichannel regulation by extracellular Ca^{2+}

A significant effect of the D50N mutation is to render hemichannels nearly insensitive to inhibition by extracellular Ca^{2+}, as initially reported by Lee et al. (2009). Macroscopic hemichannel currents differed only modestly in magnitude in bath solutions with no added Ca^{2+} compared with 5 mM Ca^{2+}. Here we also quantified Ca^{2+} effects at various voltages and found loss of inhibition over a wide, physiological voltage range, −80 to 40 mV. Two other KID mutants in E1, A40V and G45E, shown for comparison (Fig. 1 C), exhibited relatively strong inhibition by Ca^{2+} but also were deficient compared with WT Cx26. In all mutants, as well as in WT Cx26, Ca^{2+} effects exhibited voltage dependence, showing less effective inhibition at positive membrane voltages. This apparent voltage dependence is derived, in large part, from the action of Ca^{2+}, which is to shift voltage-dependent activation as discussed in the next section.

Ca^{2+} and the D50N mutation alter the chemical component of the energy change associated with hemichannel opening

Mechanistically, extracellular divalent cations selectively modulate loop gating (Verselis and Srinivas, 2008), one of two forms of voltage-dependent gating expressed in Cx GJ channels and hemichannels (Bukauskas and Verselis, 2004). Loop gating activates hemichannels with membrane depolarization, and the primary effect of divalent cations, principally Ca^{2+}, is to strongly shift activation positive, with modest, if any, effects on the steepness of voltage dependence (Ebihara and Steiner, 1993; Verselis and Srinivas, 2008; Sánchez et al., 2010). The shift in activation, reflected in the calculated $V_{1/2}$, is in the order of 60–70 mV when comparing 0 (nominal) and 2 mM Ca^{2+}. Thus, the binding of Ca^{2+} significantly affects the chemical component of the energy change associated with hemichannel opening and closing. There is a decrease in maximal conductance in high Ca^{2+} as well, which may be caused by some effect on unitary conductance and the fact that the loop gate activates at voltages that now begin to affect the other

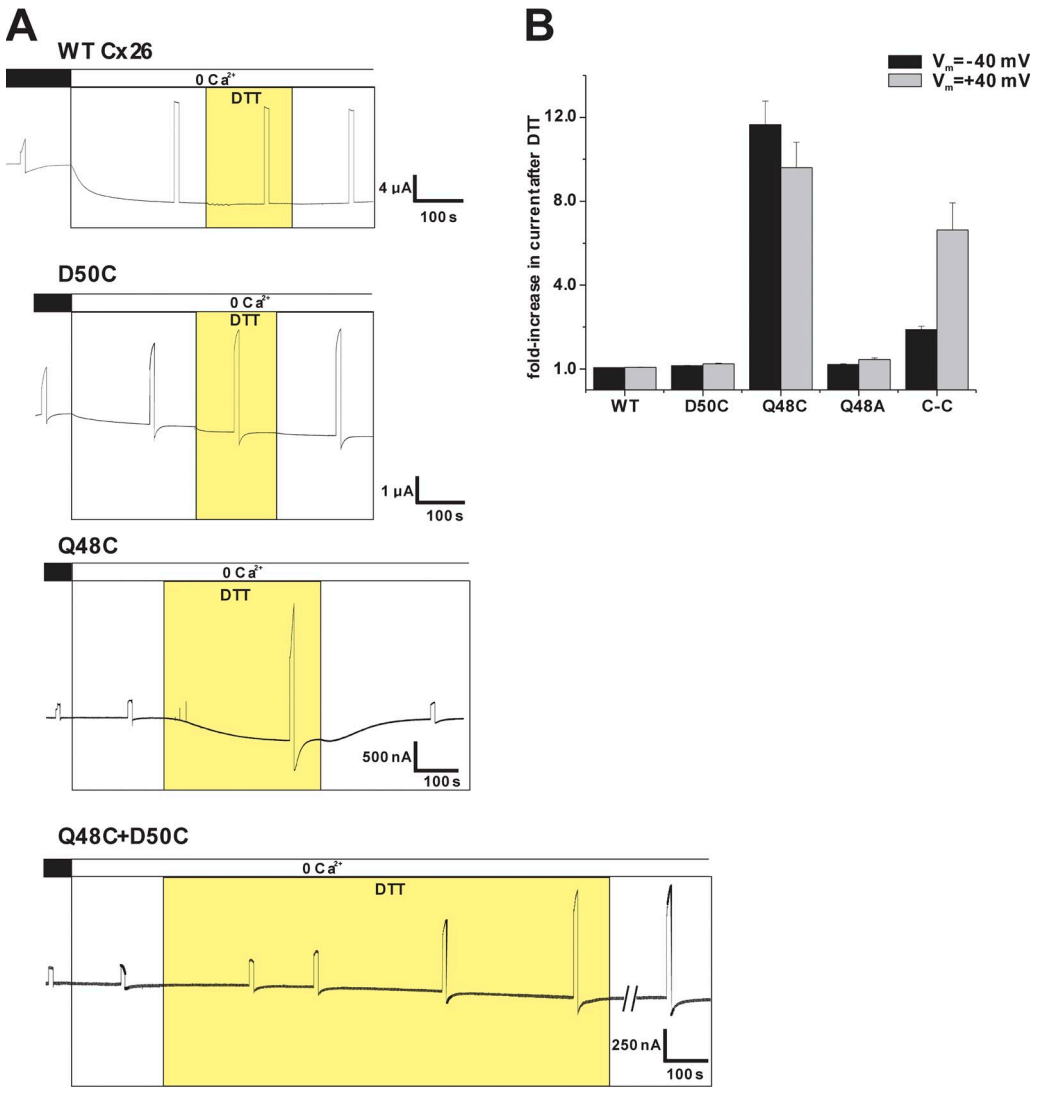

Figure 10. Effects of DTT on Cys-substituted hemichannels. (A) Representative records of membrane currents in oocytes voltage clamped at −40 mV. Voltage was occasionally stepped to 40 mV for 10 s to test for hemichannel activation. Application of 1 mM DTT (yellow) produced a large increase in current in oocytes expressing Q48C and the double mutant D50C + Q48C (bottom two panels). The effect of DTT was readily reversible after wash-out only for Q48C. DTT had essentially no effect on WT and D50C hemichannels (top two panels). (B) Bar graph summarizing the effects of DTT on WT Cx26, D50C, Q48C, and Q48C + D50C (C-C). Ala substitution at Q48 is also included. For each oocyte, current magnitude was measured at −40 and 40 mV before and after DTT. Data are plotted as fold increase in current after DTT. n = 13 for WT Cx26, 11 for D50C, 14 for Q48C, 7 for Q48A, and 7 for D50C + Q48C. Error bars represent mean ± SE.

gate, termed the fast or V_j gate, which in Cx26 closes at inside positive voltages.

Because the G-V relations are a mix of conductance changes caused by gating and open hemichannel rectification, we used the S4SM fitting algorithm (Paulauskas et al., 2009) to extract the gating parameters, $V_{1/2}$ and z. In 0 mM (nominal) Ca^{2+}, $V_{1/2}$ was shifted substantially positive (∼30 mV) for D50A and Q48A. For z values, there was an increase in WT Cx26 hemichannels in 2 mM Ca^{2+}, but values were similar in 0 mM (nominal) Ca^{2+} in all the mutants (Table 1) whether D50 was present (WT and Q48A) or absent (D50A and Q48A + D50A). Thus, loop gating remains strong and similar in its response to changes in voltage, albeit shifted along the voltage axis, irrespective of the degree of Ca^{2+} regulation. Collectively, these data suggest that D50 does not contribute significantly to the gating charge in hemichannels but does significantly affect the chemical component of the energy change associated with hemichannel opening mediated by loop gating, similar to effects of extracellular Ca^{2+}. The identities of the charges that move during loop gating remain unknown, but molecular studies have suggested that pore-lining residues in E1, near the border of TM1, move during gating (Tang et al., 2009; Verselis et al., 2009). Recent molecular dynamic simulations of the Cx26 atomic structure suggest putative open and closed states that involve a complex rearrangement of charged residues,

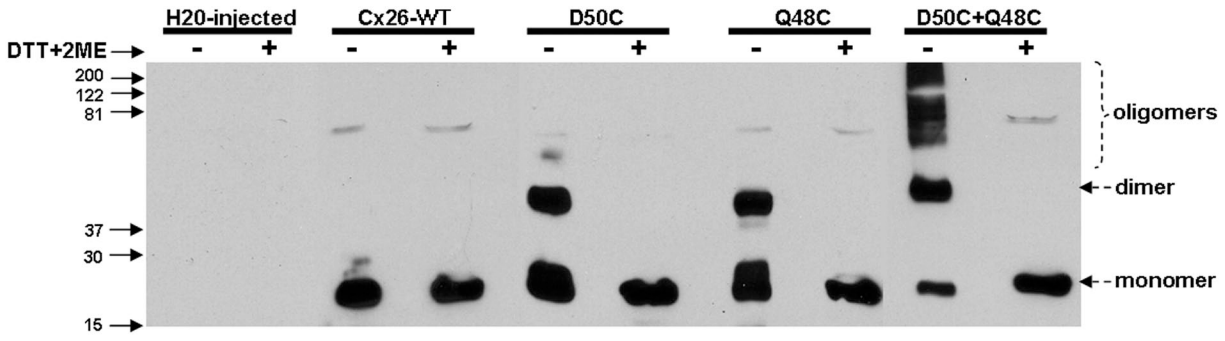

Figure 11. Q48C and D50C can form disulfide bonds between adjacent subunits. Western blots generated from samples of unpaired oocytes injected with mRNA for WT Cx26, D50C, Q48C, and D50C + Q48C. Samples were run in nonreducing (−) and reducing conditions (+) in which DTT and ME were added. Single Cys substitutions (D50C and Q48C) presented monomers and dimers; the latter was sensitive to reducing agents. However, double Cys mutant (D50C + Q48C) presented multimers, also sensitive to reducing agents, consistent with disulfide bond formation between multiple subunits. Molecular mass is indicated in kilodaltons.

as well as their interactions, residing in the TM1/E1 region (Kwon et al., 2012, 2013). Although Q48 and D50 mutations both produced shifts in activation, only D50 mutations strongly impaired Ca^{2+} regulation. Thus, D50 appears to be a critical element of the full conformational change induced by the binding of Ca^{2+}.

D50 and the possible role of intersubunit interactions in gating and Ca^{2+} regulation

An intriguing possibility we addressed for explaining the Ca^{2+} and gating effects caused by D50N comes from the crystal structure, which shows D50 plausibly involved in intersubunit interactions. Such interactions could help stabilize open or closed conformations, and disruptions of these interactions could contribute to the shifts in activation. In the crystal structure, the two residues that are putative interacting partners with D50, K61 and Q48, are part of a larger cluster of interacting residues in the TM1/E1 region (Maeda et al., 2009). We discuss our findings for each putative interacting pair separately.

K61 and D50. If the breaking of a D50–K61 salt bridge was underlying the effects of D50N on gating and Ca^{2+} regulation, then mutating either D50 or K61 would have had the same effect. However, mutation of K61 to Ala led to loss of hemichannel function. Furthermore, D50 exerts a strong electrostatic influence on ion flux in the open state of the hemichannel, consistent with its existence as a free carboxylate ion positioned in the permeation pathway and inconsistent with a D50–K61 salt bridge that would effectively neutralize D50. Although a salt bridge could form in the closed state, mutation of D50 to prevent such a salt bridge should lead to destabilization of the closed state. However, D50N hemichannels displayed no change or, if anything, even longer (stabilized) closings and shorter openings (Fig. 5). Collectively, these data suggest that K61 plays a role critical in hemichannel function, but not as an interaction partner with D50. In the crystal structure, K61 resides on a short helix toward the carboxyl end of E1 and is positioned close to F51 in the same subunit by a twist and a turn in E1 produced by a C_{53}NTLQPGC$_{60}$ sequence, perhaps stabilized by the C_{53}-C_{60} disulfide bond. Thus, it may be that this short helix plays an important role in positioning the E1 loop in such a way that allows hemichannels to function.

TABLE 2

Comparison of HC and GJC function

Cx26	HC	HC + DTT	GJC
WT	+ (349 pS)	+	+ (150 pS)
D50N	+ (167 pS)	+	−
D50A	+ (162 pS)	+	−
D50C	+ (172 pS)	+	−
K61A	−	−	+ (210 pS)
K61C	−	−	+ (200 pS)
Q48A	+ (ND)	+	+ (151 pS)
Q48C	−	+	+ (154 pS)
Q48A + D50A	+ (ND)	+	+
Q48C + D50C	−	+	+/−

GJC, GJ channel; HC, hemichannel; ND, not determined because of low expression.

Although we did not observe hemichannel currents for K61A or K61C, we observed robust currents when either of these mutants was coexpressed with WT Cx26 or D50N. When coexpressed with D50N, the currents differed from D50N expressed alone by exhibiting sensitivity to extracellular Ca^{2+}, indicating D50N and K61C/A subunits had formed heteromeric hemichannels and that the K61C/A subunits conferred Ca^{2+} sensitivity. Formation of heteromers was also evident in recordings of single hemichannels, which showed varying conductance and rectification properties intermediate between D50N and WT Cx26. When K61C was coexpressed with WT Cx26, unitary conductance and rectification were similar to WT Cx26 (unpublished data). Application of MTS reagents to the heteromeric hemichannels containing K61C did not produce any

noticeable effects in unitary conductance or rectification. From these data, we can infer that K61 mutant subunits retain WT Cx26 open hemichannel properties and that K61 is not exposed to the pore, at least in hemichannels. This view conflicts with the crystal structure of the Cx26 GJ channel that positions K61 in the pore.

When we injected D50N and K61C mRNAs in a ratio of 1:4 D50N:K61C, the binomial probability predicts ∼65% of the hemichannels will contain five or six K61C subunits. However, most of the recorded single hemichannels were skewed toward D50N conductance. Thus, it may be that hemichannels incorporating K61C subunits can only function if there are sufficient D50N subunits present, suggesting a plausible requirement that a K61C subunit have a neighboring D50N or WT Cx26 subunit. In this view, the extracellular loops from neighboring subunits interact to coordinate hemichannel opening. The inability of K61A/C to function as a homomeric hemichannel is not a consequence of trafficking to the membrane because pairing cells expressing these mutants readily leads to GJ channel formation, as we discuss below.

It is important to consider that the crystal structure of Cx26 represents a GJ channel, not a hemichannel. Relevant to this point, K61 substitutions functioned as GJ channels but not as hemichannels. Interestingly, the unitary conductances of the K61 mutants were higher than WT Cx26 GJ channels (Table 2). Whether this increased unitary conductance results from a direct effect of K61 as a pore residue in GJ channels or some indirect, allosteric effect is unknown. If exposed to the pore in the GJ channel configuration, K61 could conceivably interact with D50. In any case, the structure in the E1 region of Cx26 appears to differ between docked and undocked hemichannel configurations in such a way that permits function of homomeric K61 mutant hemichannels only in the docked configuration. Given that the crystal structure of the GJ channel and our SCAM data on hemichannels both agree that D50 is pore lining, there is clearly gross conservation of E1 structure between the two configurations, notwithstanding differences that appear to exist that alter the positions of residues, like K61, sufficient to affect exposure to the pore or participation in inter- and intrasubunit interactions.

Q48 and D50. We provide evidence, both electrophysiological and biochemical, that Q48 can participate in an intersubunit interaction with D50. Mutation of either Q48 or D50 to an Ala residue produced a positive shift in loop gating in low Ca^{2+}, and mutant cycle analysis indicated a stronger interaction energy between Q48A and D50A in low Ca^{2+}. Western blots using Cys substitutions at these positions in nonreducing conditions showed evidence of multimer formation consistent with a direct interaction between D50C and Q48C from adjacent subunits. Thus, part of the action of Ca^{2+} could include a disruption of a Q48–D50 interaction, leading to a positive shift in loop gating. However, the breaking of this interaction cannot explain the magnitude of the shift in activation caused by Ca^{2+} in WT Cx26 hemichannels, as well as the fact that Q48A hemichannels, although lacking the interaction and exhibiting a positive shift with no added Ca^{2+}, continue to shift with the addition of Ca^{2+}. Moreover, the expectation for the double Q48C + D50C mutant, in which a Q48C–D50C interaction can become covalent, would be a G-V relation with activation fixed at a hyperpolarized voltage, i.e., locked in an interaction. Instead, the hemichannels were closed or nonfunctional without DTT. Thus, it is possible that an interaction between Q48 and D50 occurs in WT Cx26, but Cys substitutions at both of these positions and subsequent disulfide bond formation distort the structure in the E1 region in such a way that impairs hemichannel function. Alternatively, it may also be that the Q48C–D50C interaction occurs during folding and membrane insertion but not once a hemichannel is opened by DTT, perhaps explaining why the disulfides do not reform readily after washout of DTT. Thus, we cannot rule out the possibility that the calculated interaction energy between Q48 and D50 deduced from mutant cycle analysis is indirect and results from interactions involving other residues in the TM1/E1 region, as suggested by the crystal structure. Molecular dynamic simulations suggest fluctuations in the electrostatic network in the TM1/E1 region across subunit boundaries may be linked to gating (Kwon et al., 2012). Thus, the complex network of interacting residues in this region of the hemichannel complicates simple interpretation of our data in involving Q48 and D50. Nonetheless, it is apparent that interactions among residues in the TM1/E1 region are important for Cx26 hemichannel function.

D50 and Ca^{2+} binding

The most straightforward explanation for the virtual insensitivity of D50N hemichannels to extracellular Ca^{2+} is that binding of Ca^{2+} is disrupted. The expectation, in this case, would be a negative shift in activation, like that characteristic of WT Cx26 hemichannels when Ca^{2+} is omitted from the bathing medium to render the binding site unoccupied. However, the shift in activation was the other way, to more positive voltages. Nonetheless, this positive shift could be a consequence of an altered structure caused by the mutation, and thus, we cannot definitively rule out a disruption of Ca^{2+} binding. However, several observations suggest that D50 may not contribute to the Ca^{2+}-binding site. We show that D50 is in the pore and that the charge at this position significantly impacts ion conduction and open hemichannel rectification. Binding of Ca^{2+} at D50 in WT Cx26 hemichannels would essentially fix divalent cations in the pore, which would severely impact ionic

flux, if not block conduction altogether. However, when exposed to high extracellular Ca^{2+}, WT Cx26 hemichannels exhibit permeability to Ca^{2+}, and the G45E KID mutant, which maintains D50, exhibits a substantial increase in Ca^{2+} permeability (Sánchez et al., 2010). Furthermore, the instantaneous I-V curve for WT Cx26, which reflects open hemichannel rectification, is similar in high and low Ca^{2+} concentrations (unpublished data). Finally, a study of Cx46 hemichannels suggests that divalent cations bind to an extracellular site and act to induce closure of the loop gate rather than block the pore (Verselis and Srinivas, 2008). Thus, we find it more likely that mutation of D50 either affects the binding of Ca^{2+} at a nearby site or acts to uncouple Ca^{2+} binding from loop gating. Based on the substitutions we examined at D50, charge at this position plays an important role, which points to an electrostatic mechanism involving either a direct influence on Ca^{2+} bound to nearby residues or on charged residues that play a critical role in conformational changes that occur with the binding of Ca^{2+}.

Cys substitutions at Q48 and D50 indicate that there is considerable flexibility in the E1 region of Cx26 hemichannels

Cys substitutions and subsequent analysis by Western blots in nonreducing conditions showed evidence that individual Q48C and D50C mutants, as well as the double Q48C + D50C mutant exhibit the capacity to form disulfides between subunits. Intersubunit disulfide bond formation was not seen in WT Cx26, D50A, or Q48A (unpublished data for the latter two), indicating that Cys substitution at position 48 or 50 was required and did not result from a generally altered structure by any substitution that subsequently resulted in inappropriate disulfide bond formation between endogenous Cys residues. Collectively, these data suggest that Q48 residues from different subunits, and likewise D50 residues, can come close enough to interact. The interactions in the single mutants appear to be homologous, i.e., Q48C with Q48C and D50C with D50C, because only dimers were evident. In contrast, multimer formation in the double Q48C + D50C mutant is consistent with a heterologous interaction, i.e., Q48C with D50C. A faint higher molecular weight band was sometimes observed in D50C alone, suggesting that a small fraction of D50C residues can form inappropriate heterologous disulfides with one of the endogenous Cys residues. However, this does not appear to be a significant fraction. We confirmed D50 to be in the hemichannel pore, and movements of subunits that narrow the pore in this region could explain homologous disulfide formation between D50C residues. The same goes for Q48C, but we could not definitively test for exposure to the pore because we could not obtain hemichannel function without DTT. Application of MTS reagents, MTSET and MTSES, to Q48C hemichannel currents during washout of DTT produced reductions in current but could have resulted from a speed-up of DTT removal; Q48C currents declined fairly rapidly simply upon washing out DTT. Nonetheless, the proximity of Q48 to D50 places Q48C near the pore and plausibly in a position to form homologous disulfides upon movements that narrow the pore in this region. Overall, there appears to be considerable flexibility in this region of the hemichannel consistent with studies of other connexins (Tang et al., 2009; Verselis et al., 2009).

As previously mentioned, disulfide bond formation detected in the Western blots may occur during folding. Also, reports have shown that reflexive junctions can form in single, unpaired oocytes between membrane microvilli as well as large invaginations of the plasma membrane (Werner et al., 1985; Zampighi et al., 1999). Thus, our biochemical data likely include both configurations of Cx26 channel. Unfortunately, we could not obtain Western blots of surface-biotinylated Cx26 in nonreducing conditions. However, our electrophysiological data showing that DTT is required in order for Q48C and Q48C + D50C hemichannels to function provides evidence that disulfides are forming in hemichannels that are operating in the plasma membrane. Although monomer bands are present in Western blots, a single dimer in a hemichannel may be sufficient to impair function. The ability of Q48C alone to interact across subunits and correspondingly show impaired function without DTT complicates interpretation of the DTT dependence of the Q48C + D50C double mutant. It may simply be that DTT dependence is a consequence of Q48C alone. However, the Q48C + D50C mutant responded much slower to DTT than the Q48C mutant and did not reverse on washout. Thus, it would appear that different disulfide bonds form in the Q48C and Q48C + D50C mutants, consistent with the Western blots that showed dimer and multimer formation, respectively. Curiously, the single D50C mutant also shows evidence of dimer formation in Western blots, but the hemichannels function without DTT and show little, if any, effect of DTT. Thus, it may be that D50C dimers form in reflexive GJ channels, albeit nonfunctional, but we cannot rule out formation in hemichannels; the latter would require that the resulting conformation supports ion conduction.

Implications for cellular dysfunction for patients carrying the D50N mutation

There is growing evidence that cellular dysfunction associated with mutations in Cx26 that cause syndromic deafness results from aberrant hemichannel activity (Stong et al., 2006; Gerido et al., 2007; Lee et al., 2009; Sánchez et al., 2010; Terrinoni et al., 2010). Loss of Cx26 GJ channel function leads to deafness but not skin disorders, an indication that loss of Cx26 GJ function is

not the cause of skin pathology in KID or other syndromic deafness patients. Moreover, it is apparent that functional contributions of Cx26 GJs differ in the cochlea and in skin. In the case of D50N, there is aberrant hemichannel function that is accompanied by a loss of GJ channel function. Thus, for D50N, it is conceivable that loss of GJ channel function contributes to deafness. In contrast, the aberrant hemichannel characteristics exhibited by D50N are likely the basis for the skin pathologies and can also contribute to or principally be responsible for deafness as the result of deleterious effects on the cochlear support cells. However, we cannot rule out that interactions of D50N with WT Cx26 or other connexins expressed in skin or the cochlea play a role in disease. The latter can involve GJs and/or hemichannels.

Interestingly, the phenotypes among the KID mutants differ substantially (Lee and White, 2009). D50N is characterized by hearing impairment that can be moderate to severe, widespread hyperkeratosis, sparse scalp hair, dystrophic nails, corneal dystrophy, and particularly severe vascularizing keratitis (Richard et al., 2002; van Steensel et al., 2002; Yotsumoto et al., 2003; Janecke et al., 2005). G45E, a KID mutation at a nearby E1 residue, exhibits one of the most severe phenotypes characterized by profound, prelingual deafness with no evidence of auditory brainstem responses and skin lesions that lead to fatality caused by uncontrollable sepsis (Janecke et al., 2005). There is also considerable dysplasia of cochlear and saccular neuroepithelium, suggesting disrupted differentiation and/or cell death may occur during development (Griffith et al., 2006). Such phenotypic differences suggests that the different KID mutations may have distinct effects on hemichannel function, and here we show that, indeed, D50N hemichannel function is altered in several ways that differ from the other KID mutants characterized thus far. D50N exhibits the most severe weakening of Ca^{2+} regulation, yet the clinical phenotypes are not correspondingly more severe. One possibility is that the positively shifted activation of loop gating in D50N tends to close the mutant hemichannels at hyperpolarized voltages, regardless of Ca^{2+} conditions. This property would be protective in the support cells of the cochlear epithelium, which exhibit robust resting potentials of −75 to −80 mV (Oesterle and Dallos, 1990; Lang et al., 2007). In contrast, keratinocytes possess less robust resting potentials, approximately −30 mV (Wohlrab et al., 2000), which could lead to more D50N hemichannel activity in skin. However, it is important to consider that D50 is a pore-lining residue. We show that removal of the six negative charges conferred by D50 has a strong impact on ion conduction in hemichannels. By inference, this also should have a strong impact on the permeabilities to signaling molecules. The G45E KID mutation, which is also a mutation of a pore-lining residue, was shown to affect hemichannel permeability, notably enhancing permeability to Ca^{2+} (Sánchez et al., 2010). Thus, it may be that D50N has the opposite effect, reducing Ca^{2+} permeability, thereby accounting for a less severe phenotype than G45E in skin even though hemichannel activity could be higher as the result of loss of inhibition by extracellular Ca^{2+}. Another important signaling molecule in cochlea and skin is ATP. In skin, persistent expression of Cx26 was shown to maintain wounded epidermis in a hyperproliferative state and to block remodeling, leading to infiltration of immune cells (Djalilian et al., 2006). In addition, the same study showed that ectopic Cx26 expression is associated with increased ATP release, resulting in delayed recovery of the epidermal barrier and promotion of an inflammatory response. The amount of ATP released would also depend on extracellular Ca^{2+} levels, which effectively close WT Cx26 hemichannels. For D50N, insensitivity to extracellular Ca^{2+} and removal of a barrier to anion flux could provide for increased release of ATP, thereby contributing specific disease characteristics.

An additional complexity in correlating Cx26 mutations with clinical phenotypes is that there are other Cxs expressed in these tissues and interactions of Cx26 mutants with these Cxs may differ in each case. However, all of the KID mutants are dominant and function as hemichannels, and thus the properties of the Cx26 mutant hemichannels are relevant. Knowledge of the mechanisms of hemichannel dysfunction should help to understand the varying disease phenotypes associated with syndromic deafness and lead to strategies for treatments.

We thank Dr. Tomitake Tsukihara for the alternative Protein Data Bank file for Cx26 and for critical reading of the manuscript. We also thank Drs. Nerius Paulauskas and Feliksas Bukauskas for their assistance with fitting data using the S4SM.

This work was supported by National Institutes of Health grants GM54179 (to V.K. Verselis) and EY013869 to (M. Srinivas). H.A. Sanchez is supported by training grant T32 NS007439.

Angus C. Nairn served as editor.

Submitted: 14 January 2013
Accepted: 24 May 2013

REFERENCES

Bukauskas, F.F., and V.K. Verselis. 2004. Gap junction channel gating. *Biochim. Biophys. Acta.* 1662:42–60. http://dx.doi.org/10.1016/j.bbamem.2004.01.008

DeCaen, P.G., V. Yarov-Yarovoy, Y. Zhao, T. Scheuer, and W.A. Catterall. 2008. Disulfide locking a sodium channel voltage sensor reveals ion pair formation during activation. *Proc. Natl. Acad. Sci. USA.* 105:15142–15147. http://dx.doi.org/10.1073/pnas.0806486105

Djalilian, A.R., D. McGaughey, S. Patel, E.Y. Seo, C. Yang, J. Cheng, M. Tomic, S. Sinha, A. Ishida-Yamamoto, and J.A. Segre. 2006. Connexin 26 regulates epidermal barrier and wound remodeling and promotes psoriasiform response. *J. Clin. Invest.* 116:1243–1253. http://dx.doi.org/10.1172/JCI27186

Ebihara, L., and E. Steiner. 1993. Properties of a nonjunctional current expressed from a rat connexin46 cDNA in *Xenopus* oocytes.

J. Gen. Physiol. 102:59–74. http://dx.doi.org/10.1085/jgp.102.1.59

Gerido, D.A., A.M. DeRosa, G. Richard, and T.W. White. 2007. Aberrant hemichannel properties of Cx26 mutations causing skin disease and deafness. *Am. J. Physiol. Cell Physiol.* 293:C337–C345. http://dx.doi.org/10.1152/ajpcell.00626.2006

Griffith, A.J., Y. Yang, S.P. Pryor, H.J. Park, E.W. Jabs, J.B. Nadol Jr., L.J. Russell, D.I. Wasserman, G. Richard, J.C. Adams, and S.N. Merchant. 2006. Cochleosaccular dysplasia associated with a connexin 26 mutation in keratitis-ichthyosis-deafness syndrome. *Laryngoscope.* 116:1404–1408. http://dx.doi.org/10.1097/01.mlg.0000224549.75161.ca

Hoang Dinh, E., S. Ahmad, Q. Chang, W. Tang, B. Stong, and X. Lin. 2009. Diverse deafness mechanisms of connexin mutations revealed by studies using in vitro approaches and mouse models. *Brain Res.* 1277:52–69. http://dx.doi.org/10.1016/j.brainres.2009.02.008

Janecke, A.R., H.C. Hennies, B. Günther, G. Gansl, J. Smolle, E.M. Messmer, G. Utermann, and O. Rittinger. 2005. GJB2 mutations in keratitis-ichthyosis-deafness syndrome including its fatal form. *Am. J. Med. Genet. A.* 133A:128–131. http://dx.doi.org/10.1002/ajmg.a.30515

Karlin, A., and M.H. Akabas. 1998. Substituted-cysteine accessibility method. *Methods Enzymol.* 293:123–145. http://dx.doi.org/10.1016/S0076-6879(98)93011-7

Kronengold, J., E.B. Trexler, F.F. Bukauskas, T.A. Bargiello, and V.K. Verselis. 2003. Single-channel SCAM identifies pore-lining residues in the first extracellular loop and first transmembrane domains of Cx46 hemichannels. *J. Gen. Physiol.* 122:389–405. http://dx.doi.org/10.1085/jgp.200308861

Kwon, T., B. Roux, S. Jo, J.B. Klauda, A.L. Harris, and T.A. Bargiello. 2012. Molecular dynamics simulations of the Cx26 hemichannel: insights into voltage-dependent loop-gating. *Biophys. J.* 102:1341–1351. http://dx.doi.org/10.1016/j.bpj.2012.02.009

Kwon, T., Q. Tang, and T.A. Bargiello. 2013. Voltage-dependent gating of the Cx32*43E1 hemichannel: Conformational changes at the channel entrances. *J. Gen. Physiol.* 141:243–259. http://dx.doi.org/10.1085/jgp.201210839

Lang, F., V. Vallon, M. Knipper, and P. Wangemann. 2007. Functional significance of channels and transporters expressed in the inner ear and kidney. *Am. J. Physiol. Cell Physiol.* 293:C1187–C1208. http://dx.doi.org/10.1152/ajpcell.00024.2007

Lee, J.R., and T.W. White. 2009. Connexin-26 mutations in deafness and skin disease. *Expert Rev. Mol. Med.* 11:e35. http://dx.doi.org/10.1017/S1462399409001276

Lee, J.R., A.M. Derosa, and T.W. White. 2009. Connexin mutations causing skin disease and deafness increase hemichannel activity and cell death when expressed in *Xenopus* oocytes. *J. Invest. Dermatol.* 129:870–878. http://dx.doi.org/10.1038/jid.2008.335

Maeda, S., S. Nakagawa, M. Suga, E. Yamashita, A. Oshima, Y. Fujiyoshi, and T. Tsukihara. 2009. Structure of the connexin 26 gap junction channel at 3.5 A resolution. *Nature.* 458:597–602. http://dx.doi.org/10.1038/nature07869

Mazereeuw-Hautier, J., E. Bitoun, J. Chevrant-Breton, S.Y. Man, C. Bodemer, C. Prins, C. Antille, J.H. Saurat, D. Atherton, J.I. Harper, et al. 2007. Keratitis-ichthyosis-deafness syndrome: disease expression and spectrum of connexin 26 (GJB2) mutations in 14 patients. *Br. J. Dermatol.* 156:1015–1019. http://dx.doi.org/10.1111/j.1365-2133.2007.07806.x

Meşe, G., E. Londin, R. Mui, P.R. Brink, and T.W. White. 2004. Altered gating properties of functional Cx26 mutants associated with recessive non-syndromic hearing loss. *Hum. Genet.* 115:191–199. http://dx.doi.org/10.1007/s00439-004-1142-6

Oesterle, E.C., and P. Dallos. 1990. Intracellular recordings from supporting cells in the guinea pig cochlea: DC potentials. *J. Neurophysiol.* 64:617–636.

Paulauskas, N., M. Pranevicius, H. Pranevicius, and F.F. Bukauskas. 2009. A stochastic four-state model of contingent gating of gap junction channels containing two "fast" gates sensitive to transjunctional voltage. *Biophys. J.* 96:3936–3948. http://dx.doi.org/10.1016/j.bpj.2009.01.059

Paulauskas, N., H. Pranevicius, J. Mockus, and F.F. Bukauskas. 2012. Stochastic 16-state model of voltage gating of gap-junction channels enclosing fast and slow gates. *Biophys. J.* 102:2471–2480. http://dx.doi.org/10.1016/j.bpj.2012.04.038

Richard, G., F. Rouan, C.E. Willoughby, N. Brown, P. Chung, M. Ryynänen, E.W. Jabs, S.J. Bale, J.J. DiGiovanna, J. Uitto, and L. Russell. 2002. Missense mutations in GJB2 encoding connexin-26 cause the ectodermal dysplasia keratitis-ichthyosis-deafness syndrome. *Am. J. Hum. Genet.* 70:1341–1348. http://dx.doi.org/10.1086/339986

Rubinos, C., H.A. Sánchez, V.K. Verselis, and M. Srinivas. 2012. Mechanism of inhibition of connexin channels by the quinine derivative *N*-benzylquininium. *J. Gen. Physiol.* 139:69–82. http://dx.doi.org/10.1085/jgp.201110678

Sánchez, H.A., G. Mese, M. Srinivas, T.W. White, and V.K. Verselis. 2010. Differentially altered Ca^{2+} regulation and Ca^{2+} permeability in Cx26 hemichannels formed by the A40V and G45E mutations that cause keratitis ichthyosis deafness syndrome. *J. Gen. Physiol.* 136:47–62. http://dx.doi.org/10.1085/jgp.201010433

Srinivas, M., M.G. Hopperstad, and D.C. Spray. 2001. Quinine blocks specific gap junction channel subtypes. *Proc. Natl. Acad. Sci. USA.* 98:10942–10947. http://dx.doi.org/10.1073/pnas.191206198

Srinivas, M., J. Kronengold, F.F. Bukauskas, T.A. Bargiello, and V.K. Verselis. 2005. Correlative studies of gating in Cx46 and Cx50 hemichannels and gap junction channels. *Biophys. J.* 88:1725–1739. http://dx.doi.org/10.1529/biophysj.104.054023

Stong, B.C., Q. Chang, S. Ahmad, and X. Lin. 2006. A novel mechanism for connexin 26 mutation linked deafness: cell death caused by leaky gap junction hemichannels. *Laryngoscope.* 116:2205–2210. http://dx.doi.org/10.1097/01.mlg.0000241944.77192.d2

Tang, Q., T.L. Dowd, V.K. Verselis, and T.A. Bargiello. 2009. Conformational changes in a pore-forming region underlie voltage-dependent "loop gating" of an unapposed connexin hemichannel. *J. Gen. Physiol.* 133:555–570. http://dx.doi.org/10.1085/jgp.200910207

Terrinoni, A., A. Codispoti, V. Serra, B. Didona, E. Bruno, R. Nisticò, M. Giustizieri, M. Alessandrini, E. Campione, and G. Melino. 2010. Connexin 26 (GJB2) mutations, causing KID syndrome, are associated with cell death due to calcium gating deregulation. *Biochem. Biophys. Res. Commun.* 394:909–914. http://dx.doi.org/10.1016/j.bbrc.2010.03.073

Trexler, E.B., M.V. Bennett, T.A. Bargiello, and V.K. Verselis. 1996. Voltage gating and permeation in a gap junction hemichannel. *Proc. Natl. Acad. Sci. USA.* 93:5836–5841. http://dx.doi.org/10.1073/pnas.93.12.5836

Trexler, E.B., F.F. Bukauskas, J. Kronengold, T.A. Bargiello, and V.K. Verselis. 2000. The first extracellular loop domain is a major determinant of charge selectivity in connexin46 channels. *Biophys. J.* 79:3036–3051. http://dx.doi.org/10.1016/S0006-3495(00)76539-8

van Steensel, M.A., M. van Geel, M. Nahuys, J.H. Smitt, and P.M. Steijlen. 2002. A novel connexin 26 mutation in a patient diagnosed with keratitis-ichthyosis-deafness syndrome. *J. Invest. Dermatol.* 118:724–727. http://dx.doi.org/10.1046/j.1523-1747.2002.01735.x

Verselis, V.K. 2009. The connexin channel pore: Pore-lining segments and residues. *In* Connexins: A Guide. A. Harris and D. Locke, editors. Humana Press, New York. 77–102.

Verselis, V.K., and M. Srinivas. 2008. Divalent cations regulate connexin hemichannels by modulating intrinsic voltage-dependent

gating. *J. Gen. Physiol.* 132:315–327. http://dx.doi.org/10.1085/jgp.200810029

Verselis, V.K., C.S. Ginter, and T.A. Bargiello. 1994. Opposite voltage gating polarities of two closely related connexins. *Nature.* 368:348–351. http://dx.doi.org/10.1038/368348a0

Verselis, V.K., M.P. Trelles, C. Rubinos, T.A. Bargiello, and M. Srinivas. 2009. Loop gating of connexin hemichannels involves movement of pore-lining residues in the first extracellular loop domain. *J. Biol. Chem.* 284:4484–4493. http://dx.doi.org/10.1074/jbc.M807430200

Werner, R., T. Miller, R. Azarnia, and G. Dahl. 1985. Translation and functional expression of cell-cell channel mRNA in *Xenopus* oocytes. *J. Membr. Biol.* 87:253–268. http://dx.doi.org/10.1007/BF01871226

White, T.W., R. Bruzzone, D.A. Goodenough, and D.L. Paul. 1992. Mouse Cx50, a functional member of the connexin family of gap junction proteins, is the lens fiber protein MP70. *Mol. Biol. Cell.* 3:711–720.

Wilders, R., and H.J. Jongsma. 1992. Limitations of the dual voltage clamp method in assaying conductance and kinetics of gap junction channels. *Biophys. J.* 63:942–953. http://dx.doi.org/10.1016/S0006-3495(92)81664-8

Wohlrab, D., J. Wohlrab, and F. Markwardt. 2000. Electrophysiological characterization of human keratinocytes using the patch-clamp technique. *Exp. Dermatol.* 9:219–223. http://dx.doi.org/10.1034/j.1600-0625.2000.009003219.x

Yifrach, O., and R. MacKinnon. 2002. Energetics of pore opening in a voltage-gated K(+) channel. *Cell.* 111:231–239. http://dx.doi.org/10.1016/S0092-8674(02)01013-9

Yotsumoto, S., T. Hashiguchi, X. Chen, N. Ohtake, A. Tomitaka, H. Akamatsu, K. Matsunaga, S. Shiraishi, H. Miura, J. Adachi, and T. Kanzaki. 2003. Novel mutations in GJB2 encoding connexin-26 in Japanese patients with keratitis-ichthyosis-deafness syndrome. *Br. J. Dermatol.* 148:649–653. http://dx.doi.org/10.1046/j.1365-2133.2003.05245.x

Zampighi, G.A., D.D. Loo, M. Kreman, S. Eskandari, and E.M. Wright. 1999. Functional and morphological correlates of connexin50 expressed in *Xenopus laevis* oocytes. *J. Gen. Physiol.* 113:507–524. http://dx.doi.org/10.1085/jgp.113.4.507